remote sensing

MDPI

Review

Affecting Factors and Recent Improvements of the Photochemical Reflectance Index (PRI) for Remotely Sensing Foliar, Canopy and Ecosystemic Radiation-Use Efficiencies

Chao Zhang [1,2,*], Iolanda Filella [1,2], Martín F. Garbulsky [3] and Josep Peñuelas [1,2]

[1] CREAF, Center for Ecological Research and Forestry Applications, Cerdanyola del Vallès, Barcelona 08193, Catalonia, Spain; iola@creaf.uab.cat (I.F.); josep.penuelas@uab.cat (J.P.)
[2] CSIC, Global Ecology Unit CREAF-CSIC-UAB, Cerdanyola del Vallès, Barcelona 08193, Catalonia, Spain
[3] Cátedra de Forrajicultura, Facultad de Agronomía, University of Buenos Aires, IFEVA/CONICET, Buenos Aires C1417DSE, Argentina; garbulsky@agro.uba.ar
* Correspondence: c.zhang@creaf.uab.cat; Tel.: +34-935-81-3355

Academic Editors: Anatoly Gitelson, Jose Moreno, Clement Atzberger and Prasad S. Thenkabail
Received: 28 June 2016; Accepted: 15 August 2016; Published: 23 August 2016

Abstract: Accurately assessing terrestrial gross primary productivity (GPP) is crucial for characterizing the climate-carbon cycle. Remotely sensing the photochemical reflectance index (PRI) across vegetation functional types and spatiotemporal scales has received increasing attention for monitoring photosynthetic performance and simulating GPP over the last two decades. The factors confounding PRI variation, especially on long timescales, however, require the improvement of PRI understanding to generalize its use for estimating carbon uptake. In this review, we summarize the most recent publications that have reported the factors affecting PRI variation across diurnal and seasonal scales at foliar, canopy and ecosystemic levels; synthesize the reported correlations between PRI and ecophysiological variables, particularly with radiation-use efficiency (RUE) and net carbon uptake; and analyze the improvements in PRI implementation. Long-term variation of PRI could be attributed to changes in the size of constitutive pigment pools instead of xanthophyll de-epoxidation, which controls the facultative short-term changes in PRI. Structural changes at canopy and ecosystemic levels can also affect PRI variation. Our review of the scientific literature on PRI suggests that PRI is a good proxy of photosynthetic efficiency at different spatial and temporal scales. Correcting PRI by decreasing the influence of physical or physiological factors on PRI greatly strengthens the relationships between PRI and RUE and GPP. Combining PRI with solar-induced fluorescence (SIF) and optical indices for green biomass offers additional prospects.

Keywords: gross primary productivity (GPP); radiation-use efficiency (RUE); photochemical reflectance index (PRI); affecting factors; spatiotemporal scales

1. Introduction

Terrestrial gross carbon uptake, expressed as gross primary productivity (GPP), and its response to climatic changes play a key role in projections of future carbon cycles and climate [1,2]. Increasing attention has been concentrated on accurately and continuously quantifying and modeling GPP over large regions and long timescales [3–5]. Observations of vegetation primary productivity in situ, and empirical [6] or process-based [1,7] models have been successfully used to estimate the global distribution of GPP. These measurements, however, rarely provide high-quality data and contain errors originating from the uncertainties of field work, which impede a comprehensive understanding of the global terrestrial carbon cycle [2,7].

Remotely sensing carbon uptake provides a unique opportunity for extending the spatial coverage of carbon fluxes [2,8–11]. The quantification of GPP variation by remote-sensing techniques is generally based on a model of radiation-use efficiency (RUE) [12,13]. This model mainly considers the absorbed photosynthetically active radiation (APAR) and the actual photochemical efficiency [12,13]. APAR has been extensively analyzed and is usually derived from vegetation indices of greenness such as the normalized difference vegetation index (NDVI) and the enhanced vegetation index (EVI) [10,14–17]. The remote sensing of RUE, however, has been less extensively analyzed, perhaps because it is influenced by many factors [10,18–20].

RUE is commonly remotely estimated using the photochemical reflectance index (PRI), which is a proxy of ecophysiological parameters linked to the competition between energy dissipation and photochemical conversion [11,18–23]. Reflectance at 531 nm rapidly decreases in response to the dissipation of excess energy by xanthophyll de-epoxidation due to an increase in zeaxanthin concentration and to chloroplast shrinkage following an increase in thylakoid ΔpH, which is insensitive to short-term changes at 570 nm [18,19]. PRI is thus defined as (R531 − R570)/(R531 + R570), where R is the reflectance and the numbers are central wavelengths of narrow bands in nanometers. The remote sensing of photosynthetic performance and plant stress has advanced considerably over the last two decades [9,11,20,24], with tower- [25], aircraft- [26,27] and satellite- [9,28–31] based PRI at both short (hours to days) and long (days to seasons) terms since Gamon, Peñuelas and Field [18] and Peñuelas et al. [19] proposed this reflectance index. The short-term change in PRI associated with the xanthophyll cycle, as proposed by Gamon et al. [18] and Peñuelas et al. [19], is able to track photosynthetic performance and RUE, the actual or maximum photochemical efficiency of photosystem II (PSII) and non-photochemical quenching (NPQ) over a wide range of species, plant functional types and nutrient levels at foliar, canopy and ecosystemic levels under various stress conditions (e.g., water shortage, nutrient levels, disease and contamination) [19,20,23,28,32–46]. PRI has also been useful for studying aquatic vegetation [47], mosses [48–50] and lichens [51]. Photosynthetic activation can be efficiently tracked by PRI, particularly during special seasonal periods of alteration such as spring recovery in coniferous [52–55], and across years in boreal deciduous forests [56], Mediterranean holm-oak forests [29] and shrubland [22]. PRI obtained from MODIS (Moderate Resolution Imaging Spectroradiometer) [25,29,56–58], AVIRIS (Airborne Visible/Infrared Imaging Spectrometer) [59] and CHRIS/PROBA (Compact High Resolution Imaging Spectrometer launched aboard the Proba satellite) [60] can also track changes in photosynthetic performance and primary productivity at larger spatial scales. The rapid changes in carbon uptake for evergreen vegetation in densely vegetated areas have been captured by PRI, but not by widely used greenness indices such as NDVI which can be saturated due to stabilized canopy greenness [20,28,39,61–63]. PRI, a narrow-band spectral index as a proxy of ecophysiological parameters based on the changes in energetic status thus provides a quick, simple, nondestructive, labor-saving and cost-efficient means of optical sampling for exploring interactions of plant-ecosystem carbon fluxes and for promisingly monitoring and mapping RUE/GPP at larger spatiotemporal scales [11,20,64–66].

Several studies, however, have shown that PRI can be affected by solar angle, illumination, canopy structure, atmosphere, pigments and soil background [10,11,20,23,54,67–75]. Additionally, the interpretation of PRI becomes more difficult for mixed species or landscapes with varying canopy fractions [76,77], although several studies have reported correlations between PRI and photosynthetic performance [34,35,78,79]. The variation in PRI also depended on the site difference caused by vegetation types and canopy structure [62,77], which generally affected the PRI-RUE relationships. Much of the long-term variation in PRI and its tracking of carbon assimilation has recently been attributed to changes in the sizes of constitutive (slow) pigment pools that also impacted long-term tracking of carbon assimilation by PRI [23,54,55,67,76]. However, such studies have not been expanded to a wide range of species and sites, so the physiological mechanism of long-term PRI variation still remains to be clearly understood. Furthermore, the not yet resolved physiological mechanism of PRI and its high sensitivity to various extraneous effects might impede the evaluation of photosynthetic

performance, when scaling up from foliar to canopy, and ultimately, landscape and global scales [24]. Even so, recent findings of links between RUE/GPP and PRI and the integration of PRI with other parameters such as foliar pigments [80], solar-induced fluorescence (SIF) [81] or vapor-pressure deficit (VPD) [77] may provide new opportunities for the continuous assessment of carbon uptake.

In a review of the literature, Garbulsky et al. [20] found that PRI was significantly correlated with RUE and other relevant ecophysiological variables across vegetation types and spatiotemporal scales. The consistent relationships with RUE-PRI at different spatiotemporal scales were summarized by synthetic analyses of publications from 1992 to 2009. The kinds of factors that control PRI variation in different plant functional types, organizational levels and temporal scales, how and the extent to which these factors control changes in PRI and how these effects can be decreased or avoided, however, remain to be clarified. An integrated and robust model for remotely sensing carbon uptake using PRI at different scales will also need to be developed for using PRI as an estimator of carbon uptake.

In this review, we analyze the main factors that drive changes in PRI and its assessment of RUE at foliar, canopy and ecosystemic levels based on the scientific literature reviewed by Garbulsky et al. [20] and on an additional review of the literature published between 2010 and 2015, and we summarize the applications of PRI for interpreting ecophysiological variables. We also describe the principal suggestions for improving the estimation of RUE and carbon uptake using PRI. The primary purpose of this study is thus to determine if PRI, a simple, optical remote-sensing index, is a good proxy of RUE at both short and long timescales from foliar to global levels.

2. Affecting Factors

We found more than 110 publications in the Science Citation Index published from 2010 to 2015 that studied remotely sensed PRI; among those, 73 studies analyzed the disparately functional mechanisms of PRI at varying spatiotemporal scales and the factors that drive PRI variation and hinder its use at longer timescales and larger regions. Here, we reviewed these affecting factors of PRI over temporal (daily and seasonal) and spatial scales (from leaves to ecosystems).

2.1. Daily Changes

2.1.1. Foliar Level

Leaves in different canopy positions with changing illumination and varying temperature have different PRI values. For example, shaded leaves had higher PRI values than sunlit leaves with higher irradiance that generated a larger xanthophyllic pigment pool and a higher potential diurnal pigment conversion [67,82,83]. In particular, illumination also led to a lower PRI toward midday [83] and a recovery in late afternoon on sunny days [76,84–87] but to a higher PRI toward midday on cloudy days [76]. PRI changed little over time with weak light [88] and did not vary with maximum photochemical efficiency (Fv/Fm) [87,89], relative water content (RWC), CO_2 assimilation or stomatal conductance under low photosynthetic photon flux density (PPFD) (<700 $\mu mol \cdot m^{-2} \cdot s^{-1}$) [90]. In contrast, PRI values decreased under light saturation, due to the generation of a photoprotective reaction, which decreased the epoxidation state (EPS) [85]. PRI was also sensitive to increased NPQ during the initial growing stages in crops and to xanthophyllic pigments during the later growing stages [91]. PRI, however, was a poor diurnal indicator of the de-epoxidation state (DEPS) in different crown levels for spruce needles, probably due to the variation in the chlorophyll/carotenoid ratio [92].

Drought [30,93], temperature stress [87,93], low nitrogen concentration [91,94], iron deficiency [95], high altitude [96], high ultraviolet A/B [97,98] and disease [99–102] can potentially induce biochemical and physiological changes (e.g., chlorophyllic and carotenoid contents, xanthophyll cycle and NPQ) and inhibit the photochemistry of PSII, thus leading to a decrease in PRI, which was more apparent in young than in mature leaves as cadmium stress increased [103]. Variations in the angle and direction of illumination [104] and instrumental FWHM (full width at half-maximum) [69] can also change the optical properties, which then influence PRI values. Gamon and Berry [67] reported that the sizes of

both the facultative xanthophyllic and constitutive pigment pools affected PRI and that the latter but not the former caused PRI to vary with canopy position; they also suggested that lutein de-epoxidation might influence PRI variability in nature. Other studies have also reported that foliar chlorophyllic and carotenoid pigment pools, which characterize the plant physiological status, contribute greatly to the variability of PRI [91,92,105], so incorporating the effects of other photosynthetic pigments is necessary to use PRI as a more accurate proxy for biophysical parameters or plant status [88,91].

2.1.2. Canopy Level

Fifteen of the publications studied the diurnal response of canopy PRI to the ecophysiological status of the vegetation and to photosynthetic performance. The status of epoxidation of the xanthophyllic cycle accounted for most of the diurnal PRI variability [76,106], especially in the early morning and afternoon [107], and short-term adaptations to varying levels of solar irradiance increased PRI variability [106]. Damm et al. [108] demonstrated the sensitivity of canopy reflectance and vegetation indices derived from spatial and spectral high-resolution data to varying irradiances, and reported that unknown direct/diffuse irradiance caused by complex interactions of surface irradiance and reflectance anisotropy accounted for up to 32% of the uncertainty of PRI for crops. Another study found that spectra were best obtained ca. 10 a.m. but that deviation from the zenith affected PRI, although the effect of the departure of 10° from the nadir view precision on PRI accuracy was acceptable [109]. Further, a high relative azimuth angle showed higher PRI values at any view zenith angles by capturing more shaded foliage and thus decreasing the effect of soil background [82,83]. In addition, PRI tracked RUE poorly when chlorophyllic concentrations during senescence were low [109] and when wheat canopies at the elongation stage were sparse [110]. In contrast, PRI values were lower for dark soil, even with dense vegetation, but estimated RUE and PSII efficiency better [62,82,110]. PRI has also been used as an indicator of salinity stress in coastal species but varied with tissue chlorides and not with pigments [111]. Some studies have also reported that soil reflectance [62], species [110], canopy structure [75,82], tree age and illumination patterns [84] complicated the interpretation of PRI. Gamon and Bond [84], however, supported the hypothesis that photosynthesis is coordinately regulated, allowing PRI to be used as an indicator of diurnal photosynthetic activity.

2.2. Seasonal Changes

2.2.1. Foliar Level

PRI is intended as a measure of the responses of a constitutive component dependent on the pigment content of leaves and on a facultative component varying on a short timescale because of the xanthophyllic cycle [67]. Hmimina et al. [86] reported foliar pigment content had a stronger impact on PRI than on the relationship with RUE at seasonal timescales and proposed a procedure for correcting PRI that clarified this pigment effect at the foliar level. PRI values during growth were lower for sunlit than shaded leaves [83,112] and were higher for dark-green than either light- or yellow-green leaves [83,87]. PSII efficiency could not be efficiently tracked by PRI in varying light intensities, seasons and leaf colors due to the influence of chlorophyll, low temperature at night or low illumination on reflectance, which inhibit the epoxidation of the xanthophyllic cycle and retain more xanthophyllic pigments [87,113]. Likewise, the tracking of seasonal levels of Chlorophyll a/b (Chl a/b) using PRI was affected by high non-photochemical dissipation from the senescence of the vegetation and drought stress in desert species during growth [114]. PRI decreased throughout the soybean growing season due to elevated ozone concentrations, which increased the protective dissipation of excess energy and decreased the foliar contents of nitrogen and chlorophyll [115,116]. PRI, however, correlated well with NPQ in evergreens during most of the year except during spring recovery after winter down-regulation [72] and throughout the stages of crop leaves unless PRI was corrected for pigment effects [88]. Similarly, EPS could not account for the variation in PRI during spring recovery [54,55]

due to the changes in the constitutive pigment pool, but not the facultative xanthophyllic cycle, which led to the primary variation of PRI during spring recovery and over the year in evergreen conifers. Hernández-Clemente et al. [117] found that changes in chlorophyllic and carotenoid concentrations caused the variation of PRI values due to the seasonal fluctuation of foliar optical signals. Similar findings were also reported for *Salix viminalis* trees [112], eggplant [88] and oak and beech trees [86], where the sizes of the pigment pools contributed to most of the PRI variability and thus limited its use for RUE estimation on long timescales. Changes in pigment concentrations due to water stress, however, could also potentially affect the seasonal variability of PRI [118–120], but these changes varied between species such as *Umbilicaria arctica* and *U. hyperborean* [118]. PRI clearly differentiated between normal and stressed holm oaks but was not very informative under a severe drought [121], and could generally detect the physiological status of water-stressed plants but was not useful for the drought-tolerant species *Elaeagnus umbellate* [122].

2.2.2. Canopy Level

Recent studies have indicated that the changes in the patterns of seasonal and inter-annual PRI were correlated with chlorophyllic and carotenoid pool sizes and structural properties [76,107,123,124]. Structural changes of the canopy caused by sustained water stress [120,123,125,126] or a varying leaf area index (LAI) [127] over the season led to PRI variability and loss of the seasonal relationship between PRI and RUE. PRI calculated from pure crown reflectance for fruit trees under different irrigation regimes varied with xanthophyllic pigment contents and not with vegetation structure or chlorophyllic content [128]. The sensitivity of PRI to physiological indicators of stress when calculated for entire canopies, however, was considerably lower for dark soil [128]. PRI has shown sensitivity to both the zenith angle and relative azimuth angle [83]. Differences in the correlations between PRI and RUE for different types of vegetation can be due to differences in the canopy structure and shadow fraction, however, when the canopy is detected from only one angle (as with MODIS) [4], highlighting the importance of the effect of the canopy structure on PRI. PRI was also sensitive to changes in the structure and physiology during the soybean growing season caused by elevated CO_2 and O_3 concentrations [127]. Canopy PRI values were higher during the growth phase than other phases [83,129] and did not efficiently track RUE variability during the ripening stage [129]. Canopy PRI values were higher on cloudy days with low irradiance than on sunny days [130], and were correlated most strongly with RUE under clear or slightly overcast skies [123]. For some vegetation such as *Elaeagnus umbellate*, a drought-tolerant invasive species, PRI decreased slightly during water stress because of the plant's special physiological and morphological characteristics [122].

2.2.3. Ecosystemic Level

MODIS and CHRIS/PROBA are common operational instruments for studying PRI at ecosystemic and regional scales [9,60,131,132]. Alterations in the angle at which satellites detect seasonal fluctuations of illumination, the shadow fraction detected by the sensor and atmospheric effects were identified as critical influences on PRI signals on a spatial scale [31,71,79,133], with the exception of some relatively uniform and dense canopy structures and a low variability of shadow fractions [71]. PRI obtained from the backscatter direction [25,60,132] nonetheless minimized the effect of shadows, and near-nadir satellite observations [79] that reduced the effects of soil background and atmospheric scattering were also optimal and improved the accuracy of RUE detection. PRI performance was improved in forward-scattering directions after replacing the PRI formulation wavelength, which indicates a possible shift in the signal of xanthophyllic de-epoxidation with the direction of detection. In contrast, Sims et al. [134] found no difference between backward and forward effects on MODIS PRI in a dense evergreen and two deciduous forest ecosystems. MODIS PRI has detected the impacts of water stress on RUE [25], but not for severe droughts [31,135]. Intra-annual changes in MODIS PRI were dependent on the composition of foliar pigments at evergreen sites and on the dynamics of canopy structure at deciduous sites [79], but a universally applicable model for correlating

ecosystemic RUE with MODIS PRI for all types of ecosystems could not be found. Vegetation indices designed to be more sensitive to chlorophyllic content explained most of the variability in GPP in a subalpine grassland ecosystem characterized by a strong seasonally dynamic GPP, and the accuracy only slightly improved by adding PRI to the model formulation [136]. The combined use of PRI and VPD was also one of the better models for estimating RUE in tropical evergreen rainforests [77].

2.3. Other Factors

Several studies have concentrated on the influence of the configuration and calibration of field spectroradiometers on PRI variation. Most spectroradiometers are designed for periodic use, but continuous measurements and the validation of remote-sensing data are needed to improve PRI accuracy and application in assessing carbon uptake [137,138]. Regular calibration and the correction of data based on the effect of nonlinearity were therefore recommended to ensure data quality [85,137,139]. Radiometric and spectral stability have high impacts on the uncertainty of PRI. The accurate measurement of near-surface spectral data can provide an important groundwork for the calibration and validation of satellite measurements [85].

3. Application

PRI has been used as an indicator of photosynthetic function at long timescales and in large areas and of carbon uptake at large scales [8,9,11,20]. We summarized various aspects of the applications of PRI based on the review by Garbulsky et al. [20]. Sixty percent of the articles published between 2010 and 2015 linked PRI to plant physiological variables (Table 1 [4,25,28,30,31,54,55,60,62,69,71,72,75–77,79,81,84–95,98,101,103,105,107,109–115,117,119–124,126,128–130,132,136,140–153]). We included only the studies that calculated PRI as (R531 − R570)/(R531 + R570) or (R570 − R531)/(R570 + R531) [18,19] to allow analysis and comparisons. The coefficients of determination (R^2) and uncharted correlations were extracted from the figures, and were analyzed and drawn using boxplots for each type of vegetation (e.g., broadleaved, coniferous and herbaceous/crop plants), timescale (daily or seasonal, i.e., changes within or across seasons) and organizational level (foliar, canopy for a single plant or a monospecific stand, or ecosystemic for a stand of mixed species). We also included the results by Garbulsky et al. [20] in our boxplots. The correlations obtained from 153 publications were thus analyzed. All variables except the six most common ecophysiological variables linked to PRI in Table 2 in Garbulsky et al. [20] were also analyzed and plotted. The overall relationships between RUE and PRI reported during the last two decades were analyzed at daily and seasonal scales and at foliar to ecosystemic levels.

Table 1. List of published studies (2010–2015) linking photochemical reflectance index (PRI) with ecophysiological variables. Specrad, spectroradiometer. Abbreviations for the ecophysiological variables: RWC, relative water content; gS, stomatal conductance; RUE, radiation-use efficiency; net CO_2 uptake, net photosynthetic rate, gross primary productivity or light-saturated photosynthesis; EPS or DEPS, epoxidation or de-epoxidation state of the xanthophylls; Fv/Fm, maximum photochemical efficiency of PSII; ΔF/Fm', effective quantum yield, actual photochemical efficiency or photochemical efficiency of photosystem II (ΦPSII); Fs, steady-state fluorescence; NPQ, non-photochemical quenching; Chl/Car or Car/Chl, chlorophyll/carotenoid or carotenoid/chlorophyll ratio; VAZ, xanthophyll-cycle pigment pools; V, violaxanthin; A, antheraxanthin; Z, zeaxanthin; L, lutein; qN, non-photochemical quenching; PPFD, photosynthetic photon flux density; fAPAR, fraction of absorbed photosynthetically active radiation; fIPARg, fraction of photosynthetically active radiation intercepted by vegetation; α_s, canopy shadow fraction; Tl-Tair, leaf minus air temperature; Tc-Ta, crown minus air temperature.

Article Order by Published Date	Year	Reference	Scale	Variance Factor	Species/Vegetation Type	Vegetation Type	Sensor	Figure #	Ecophysiological Variable
3	2010	(Ibaraki et al. [140])	Leaves	Diurnal	Strawberry, lettuce and potato	Herbaceous and crop	PRI imaging system	1a	ΔF/Fm'
2	2010	(Ibaraki and Gupta [89])	Leaves	Diurnal	Potato	Herbaceous and crop	PRI imaging system	2	Fv/Fm
35	2013	(Kováč et al. [92])	Leaves	Diurnal	Norway spruce (*Picea abies*)	Conifers	Spectrad	1e	Chl/Car
38	2013	(Peñuelas et al. [141])	Leaves	Diurnal	*Populus nigra* and *Quercus ilex*	Broadleaf	Spectrad	2	Monoterpene emission rates Isoprene emission rates
48	2014	(Magney et al. [91])	Leaves	Diurnal	Sunflower, wheat, *Quercus macrocarpa*, *Betula papyrifera*, and *Populus tremuloides*	Herbaceous and crop and Broadleaf	Spectrad	1c 1b	NPQ DEPS
58	2016	(Harris et al. [112])	Leaves	Diurnal	*Salix viminalis*	Broadleaf	Specrad	1d and 9	RUE
								1f	Net CO_2 uptake
								1e	Car/Chl
								2	Isoprene emission rates VAZ Neoxanthin Lutein Chl Car VAZ/Chl
63	2015	(Stratoulias et al. [142])	Leaves	Diurnal	Shore reed	Herbaceous and crop	Specrad	2	Chl Fs Fm' ETR
43	2014	(Ainsworth et al. [115])	Leaves	Diurnal (Ozone)	Soybean	Herbaceous and crop	Specrad	2	Leaf N (%) Chl Seed Yield
55	2014	(Xue et al. [103])	Leaves	Diurnal (Cd polution)	Soybean	Herbaceous and crop	Specrad	1d and 9	RUE
								1f	Net CO_2 uptake
								1a	ΔF/Fm'
64	2015	(Su et al. [95])	Leaves	Diurnal (Fe deficiency)	Peanut	Herbaceous and crop	Specrad	1d and 9	RUE
								1f	Net CO_2 uptake

Table 1. *Cont.*

Article Order by Published Date	Year	Reference	Scale	Variance Factor	Species/Vegetation Type	Vegetation Type	Sensor	Figure #	Ecophysiological Variable
40	2013	(Sun et al. [143])	Leaves	Diurnal (Genetic transformation)	Barley	Herbaceous and crop	Spectrad	1d and 9	RUE
								1f	Net CO_2 uptake
21	2012	(Osório et al. [93])	Leaves	Diurnal (Moisture and temperature stress)	*Ceratonia siliqua*	Broadleaf	Spectrad	1a	ΔF/Fm′
								1c	NPQ
								2	RWC Water potential
25	2012	(Shrestha et al. [94])	leaves	Diurnal (N supply)	Rice	Herbaceous and crop	PlantPen PRI 200	1c	NPQ
37	2013	(Pallozzi et al. [98])	Leaves	Diurnal (UVA stress)	*Populus Canadensis*	Broadleaf	Spectrad	1d and 9	RUE
								1f	Net CO_2 uptake
								1a	ΔF/Fm′
30	2013	(Calderón et al. [101])	Leaves	Diurnal (Vericillium wilt)	Olive orchard	Broadleaf	PlantPen	2	Tc-Ta gS
7	2010	(Sarlikioti et al. [90])	Leaves	Diurnal (Water stress)	Tomato	Herbaceous and crop	PlantPen PRI 200	1f	Net CO_3 uptake
								2	RWC gS
8	2010	(Shahenshah et al. [144])	Leaves	Diurnal (Water stress)	Cotton and Peanut	Herbaceous and crop	PMA-11	1a	ΔF/Fm′
								1c	NPQ
13	2011	(Garrity et al. [105])	Leaves	Diurnal (Water stress)	Bur oak and 10 sugar maple	Broadleaf	Specrad	1e	Car/Chl
								2	Chl Car
18	2011	(Ripullone et al. [30])	Leaves	Diurnal (Water stress)	*Arbutus unedo*, *Quercus ilex*, *Quercus pubescens*, *Quercus cerris*, *Quercus robur*, *Cannabis sativa*, *Fagus sylvatica* and *Populus euroamericana*	Broadleaf	Specrad	1d and 6	RUE
								1f	Net CO_2 uptake
								1a	ΔF/Fm′
								1b	DEPS
								2	Water potential
27	2012	(Weng et al. [113])	Leaves	Diurnal/ Seasonal	*Pinus taiwanensis*, *Stranvaesia niitakayamensis*, two *Miscanthus* spp. and mango	Broadleaf, conifers and Herbaceous and crop	Spectrad	1a and 3a	ΔF/Fm′
								4	Fv/Fm
23	2012	(Rahimzadeh-Bajgira et al. [88])	Leaves	Diurnal/ Seasonal	*Solanum melongena*	Herbaceous and crop	Spectrad	1c	NPQ
								4a	ΔF/Fm′
								2 and 4	ETR
67	2015	(Wong and Gamon, [55])	Leaves	Diurnal/Seasonal/ Internnual	*Pinus contorta* and *Pinus ponderosa*	Conifers	Specrad	3e	Car/Chl
								3b	EPS

Table 1. *Cont.*

Article Order by Published Date	Year	Reference	Scale	Variance Factor	Species/Vegetation Type	Vegetation Type	Sensor	Figure #	Ecophysiological Variable
11	2010	(Weng et al. [87])	Leaves	Diurnal/ Seasonal	Mango	Broadleaf	Specrad	1a and 3a	ΔF/Fm′
								3b	EPS
								4	Fv/Fm Minimum temperature
46	2014	(Harris et al. [85])	Leaves/ Canopy	Diurnal	*Pinus contorta*	Conifers	Specrad	1b and 5b	EPS
32	2013	(Gamon and Bond [84])	Leaves/ Canopy	Diurnal	Douglas-fir and ponderosa pine	Conifers	Spectrad	6	PPFD
16	2011	(Hernández-Clemente et al. [69])	Leaves/ Canopy	Diurnal (Water stress)	*Pinus sylvestris* and *Pinus nigra*	Conifers	Specrad AHS airborne	1b and 5b	EPS
								6	gS Water potential
22	2012	(Porcar-Castell et al. [72])	Leaves	Seasonal	*Pinus sylvestris*	Conifers	Spectrad	3d and 9	RUE
								3c	NPQ
								3a	ΔF/Fm′
								3e	Car/Chl
								3b	DEPS
								4	Fv/Fm Car Chl VAZ VAZ/Chl
47	2014	(Hmimina et al. [86])	Leaves	Seasonal	*Quercus robur* and *Fagus sylvatica*	Broadleaf	Specrad	3d, 9 and 10a	RUE
								3a	ΔF/Fm′
60	2015	(Nyongesah et al. [114])	Leaves	Seasonal	*Haloxylon ammodendron*	Shrubland	Specrad	4	Chl a/b
62	2015	(Šebela et al. [145])	Leaves	Seasonal (High night temperature)	Rice	Herbaceous and crop	Specrad	3a	ΔF/Fm′
								4	Fs
53	2014	(Sun et al. [119])	Leaves	Seasonal (Interannual)	Olive	Broadleaf	Specrad	3d and 9	RUE
								3f	Net CO_2 uptake
								3e	Car/Chl
								4	Car RWC
54	2014	(Tsonev et al. [121])	Leaves	Seasonal (Water stress)	*Quercus ilex*	Broadleaf	Specrad	3d and 9	RUE
								3f	Net CO_2 uptake
								4	RWC

Table 1. *Cont.*

Article Order by Published Date	Year	Reference	Scale	Variance Factor	Species/Vegetation Type	Vegetation Type	Sensor	Figure #	Ecophysiological Variable
10	2010	(Suárez et al. [128])	Leaves/ Canopy	Seasonal	Peach, nectarine and orange	Broadleaf	Specrad Airborne	3b and 7b	EPS
19	2012	(Hernández-Clemente et al. [117])	Leaves/ Canopy	Seasonal	*Pinus sylvestris*	Conifers	Camera	3e	Car/Chl
								4	Car Chl
66	2015	(Wong and Gamon [54])	Leaves/ Canopy	Seasonal	*Pinus contorta*, *Pinus ponderosa* and *Picea glauca*	Conifers	Specrad	3f	Net CO_2 uptake
								3b	EPS
								3a	ΔF/Fm′
								3e	Car/Chl
								4	ETR Z/Chl L/Chl β-carotene/Chl VAZ/Chl
36	2013	(Liu et al. [110])	Canopy	Diurnal	Maize and winter wheat	Herbaceous and crop	Spectrad	5d and 9	RUE
								5f	Net CO_2 uptake
								5c	NPQ
29	2012	(Zinnert et al. [111])	Canopy	Diurnal (Salinity stress)	*Baccharis Halimifolia* and *Myrica cerifera*	Broadleaf	Spectrad	5d and 9	RUE
								5f	Net CO_2 uptake
								5a	ΔF/Fm′
								5c	NPQ
								6	gS Water potential Total chlorides
44	2014	(Delalieux et al. [146])	Canopy	Diurnal (Water stress)	Citrus orchard	Herbaceous and crop	APEX	6	Water potential
57	2015	(Gamon et al. [76])	Canopy	Diurnal/ Seasonal	*Pinus contorta*	Conifers	SRS sensor	5b	EPS
								7c	Chl/Car
4	2010	(Mänd et al. [62])	Canopy	Diurnal	*Calluna vulgaris*, *Vaccinium myrtillus*, *Empetrum nigrum*, *Populus alba*, *Erica multiflora*, *Globularia alypum*, *Cistus monspeliensis* and *Pistacia lentiscus*	Mixture	Specrad	5a	ΔF/Fm′
								6	Fv/FmqN
12	2010	(Wu et al. [109])	Canopy	Diurnal	Wheat	Herbaceous and crop	Specrad	5d, 9 and 10a	RUE
								5f	Net CO_2 uptake
61	2015	(Rossini et al. [147])	Canopy	Diurnal	Maize	Herbaceous and crop	Airborne	5a	ΔF/Fm′
								6	gS

Table 1. *Cont.*

Article Order by Published Date	Year	Reference	Scale	Variance Factor	Species/Vegetation Type	Vegetation Type	Sensor	Figure #	Ecophysiological Variable
28	2012	(Zarco-Tejada et al. [120])	Canopy	Diurnal (Water stress)	Orange and mandarin	Broadleaf	PlantPen SKR 1800 camera	6	gS Water potential
41	2013	(Zarco-Tejada et al. [75])	Canopy	Diurnal (Water stress)	Vineyard	Herbaceous and crop	Airborne	6	gS Water potential
50	2014	(Panigada et al. [148])	Canopy	Diurnal (Water stress)	Maize and sorghum	Herbaceous and crop	AISA Eagle	5a	ΔF/Fm′
26	2012	(Stagakis et al. [126])	Canopy	Diurnal/ Seasonal (Water stress)	Orange	Broadleaf	Camera	6	Water potential
5	2010	(Naumann et al. [122])	Canopy	Seasonal	*Elaeagnus umbellata*	Broadleaf	Specrad	7a	ΔF/Fm′
42	2013	(Zarco-Tejada et al. [149])	Canopy	Seasonal	Olive orchard	Broadleaf	Airborne	7e	Net CO_2 uptake
59	2015	(Hmimina et al. [107])	Canopy	Seasonal	*Quercus robur*, *Fagus sylvatica* and *Pinus sylvestris*	Mixture	Specrad	7d, 9 and 10a	RUE
65	2015	(van Leeuwen et al. [130])	Canopy	Seasonal	Douglas-fir	Conifers	PRiAnalyze	7d and 9	RUE
6	2010	(Rossini et al. [129])	Canopy	Seasonal	Rice	Herbaceous and crop	Specrad	7d and 9	RUE
								7e and 10c	Net CO_2 uptake
39	2013	(Rossini et al. [150])	Canopy	Seasonal (Water stress)	Maize	Herbaceous and crop	Airborne	7a	ΔF/Fm′ RWC Tl-Tair
1	2010	(Hilker et al. [4])	Canopy	Seasonal (Interannual)	Douglas-fir and Aspen	Broadleaf and Conifers	Specrad	7d and 9	RUE
									α_s
15	2011	(Hall et al. [151])	Canopy	Seasonal (Interannual)	Douglas-fir and Aspen	Broadleaf and Conifers	CHRIS/ PROBA		RUE
31	2013	(Cheng et al. [81])	Canopy	Seasonal (Interannual)	Corn	Herbaceous and crop	Spectrad	7d, 9 and 10b	RUE
								7e and 10c	Net CO_2 uptake
68	2015	(Wu et al. [124])	Canopy	Seasonal (Interannual)	Wheat	Herbaceous and crop	Specrad	7d, 9 and 10a	RUE
52	2014	(Stagakis et al. [60])	Leaves/ Ecosystem	Seasonal	*Phlomis fruticosa* forest	Broadleaf	Specrad CHRIS/ PROBA	3d, 8a and 9	RUE
34	2013	(Kefauver et al. [152])	Ecosystem	Ozone	*Pinus ponderosa*, *Pinus jeffreyi* and *Pinus uncinata*	Conifers	AVIRIS and CASI		O_3
56	2015	(Balzarolo et al. [153])	Ecosystem	Seasonal	grassland	Herbaceous and crop	Specrad	8a and 9	RUE
								8b	Net CO_2 uptake
24	2012	(Rossini et al. [136])	Ecosystem	Seasonal	Subalpine grassland	Herbaceous and crop	HIS	8a and 9	RUE
								8b and 10c	Net CO_2 uptake
									Chl fIPARg

Table 1. *Cont.*

Article Order by Published Date	Year	Reference	Scale	Variance Factor	Species/Vegetation Type	Vegetation Type	Sensor	Figure #	Ecophysiological Variable
9	2010	(Stagakis et al. [132])	Ecosystem	Seasonal (Interannual)	*Phlomis fruticosa* forest	Broadleaf	CHRIS/ PROBA		Chl Chl a Car Water potential
45	2014	(Guarini et al. [25])	Ecosystem	Seasonal	*Quercus cerris* forest	Broadleaf	MODIS	8a and 9	RUE
14	2011	(Goerner et al. [79])	Ecosystem	Seasonal (Interannual)	Savanna (*Combretum apiculatum*, *Sclerocarya birrea* and *Acacia nigrescens*), *Pinus ponderosa* forest, deciduous broad-leaved forest and *Quercus ilex* forest	Broadleaf and Conifers	MODIS	8a and 9	RUE
									fAPAR
20	2012	(Moreno et al. [31])	Ecosystem	Seasonal (Interannual)	Mediterranean *Pinus pinaster* forests	Conifers	MODIS	8a and 9	RUE
17	2011	(Hilker et al. [71])	Ecosystem	Seasonal (Interannual)	*Pseudotsuga Menziesii*, *Thuja plicata*, *Tsuga heterophylla*, *Quercus rubra*, *Acer rubrum*, *Betula lenta*, *Pinus strobes*, *Tsuga Canadensis*, *Pinus banksiana*, *Picea rubens*, *Picea mariana*, *Pinus banksiana*, *Eucalyptus delegatensis* and *Eucalyptus dalrympleana*	Mixture	CHRIS/ PROBA		α_s
49	2014	(Nakaji et al. [77])	Ecosystem	Seasonal (Interannual)	Dipterocarp forest (many species)	Mixture	Specrad	8a, 9 and 10b	RUE
51	2014	(Soudani et al. [123])	Ecosystem	Seasonal (Interannual)	Deciduous forest (*Quercus robur* and *Quercus petraea*) and Mediterranean evergreen forest (*Quercus ilex*)	Broadleaf	SKR 1800	8a, 9 and 10a	RUE
								8b	Net CO_2 uptake
									aPAR VPD
33	2013	(Garbulsky et al. [28])	Ecosystem	Seasonal/ Interannual	*Quercus ilex*	Broadleaf	MODIS	8a and 9	RUE
								8b	Net CO_2 uptake
									Diametric-increment

3.1. Foliar Level

3.1.1. Diurnal Changes

A total of 33 articles published from 1992 to 2015 analyzed the relationships between foliar-level PRI and actual photochemical efficiency (ΔFv/Fm'), NPQ, the chlorophyll/carotenoid ratio, EPS, DEPS, RUE or net CO_2 uptake (Figure 1). The correlations between PRI and ΔFv/Fm' (n = 57, n is the number of the correlations reported in the literature) and RUE (n = 28) were among the most relevant. Most of the relationships were focused on broadleaved and herbaceous/crop plants. The correlations for broadleaved and coniferous plants were stronger than those for herbaceous/crop plants, except for the correlations between PRI and EPS (or DEPS). R^2 for all variables other than the chlorophyll/carotenoid ratio also showed high differentiation for herbaceous/crop plants (Figure 1). PRI for broadleaved species represented medians of 80%, 76% and 78% of the variability of ΔFv/Fm', RUE and net CO_2 uptake, respectively (Figure 1a,d,f).

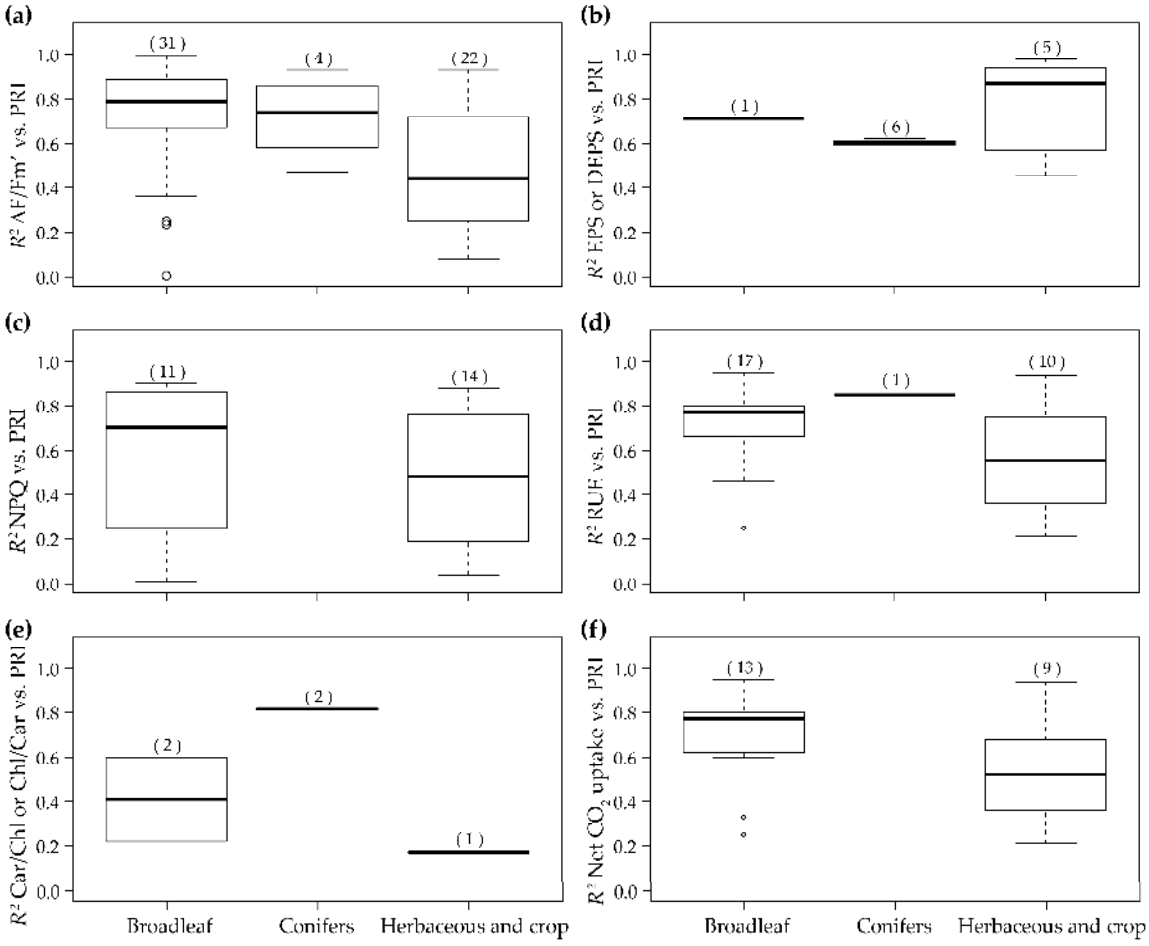

Figure 1. Boxplots of the coefficients of determination of the relationships between PRI and physiological variables at the foliar level and diurnal timescale: (**a**) Actual photochemical efficiency (ΔF/Fm'); (**b**) Epoxidation or de-epoxidation state of xanthophylls (EPS or DEPS); (**c**) Non-photochemical quenching (NPQ); (**d**) Radiation-use efficiency (RUE); (**e**) Carotenoid/chlorophyll (Car/Chl) or chlorophyll/carotenoid (Chl/Car) ratio; and (**f**) Net CO_2 uptake. Central lines represent medians, boxes represent 50% of the data, whiskers represent minima and maxima and circles represent outliers. The numbers of correlations reported in the literature are shown in brackets.

The R^2 of PRI with other physiological variables is presented in Figure 2. All studies focused on broadleaved and herbaceous/crop plants, for which PRI explained averages of 68% or 67%, respectively,

of the variation of emissions of volatile organic compounds (monoterpenes and isoprenes). PRI was significantly correlated with foliar nitrogen content and seed yield (R^2 = 0.29, $p < 0.0001$ and R^2 = 0.30, $p < 0.0001$, respectively) [115] for soybean leaves exposed to elevated ozone. PRI was also significantly correlated in six broadleaved species with water potential under water stress ($0.60 < R^2 < 0.95$) [30] and with RWC (R^2 = 0.32) under water and temperature stress [93].

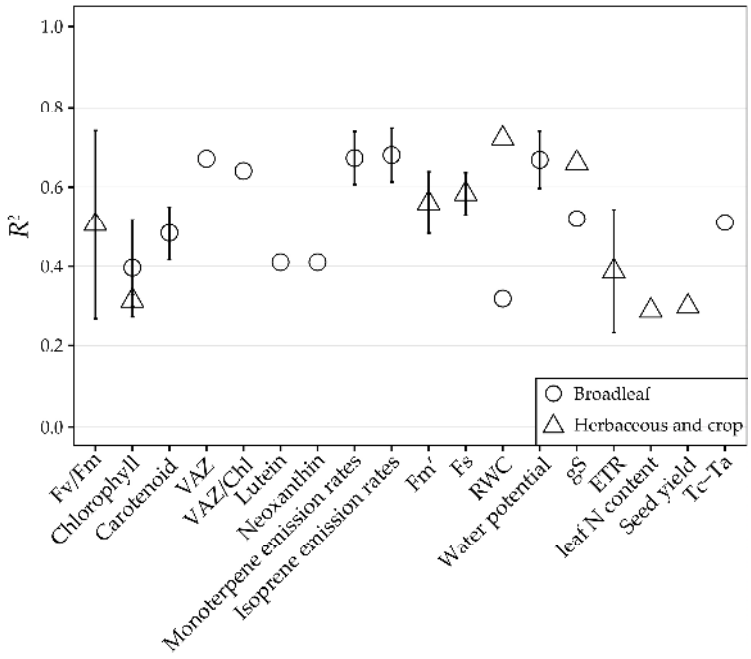

Figure 2. The mean values of coefficients of determination of the relationships between PRI and several physiological variables at the foliar level and short daily timescale. All the correlations were significant ($p < 0.05$). Error bars indicate standard error.

3.1.2. Seasonal Changes

Thirty articles published since 1992 linked PRI with ecophysiological changes at the seasonal scale (Figure 3). PRI was most often correlated with actual photochemical efficiency ΔFv/Fm' (n = 57) and explained 17%–90% of its variability (Figure 3a). Median R^2 was higher for conifers than for other species groups. PRI accounted for 0%–86% of the variability of NPQ for broadleaved and coniferous trees (Figure 3c) and was more strongly correlated with the chlorophyll/carotenoid ratio (R^2 between 0.55 and 0.89) than with EPS (or DEPS) (Figure 3b,e). The correlations between PRI and RUE and net CO_2 uptake for broadleaved species were highly variable (R^2 ranged from 0.0 to 0.84 and 0.0 to 0.92, respectively; Figure 3d,f), but median R^2 was 0.12 and 0.19 higher, respectively, than those reported by Garbulsky et al. [20].

PRI was significantly correlated with other pigments or pigment ratios (e.g., chlorophyll, xanthophyll-cycle pigment pools: chlorophyll (VAZ/Chl) and lutein/chlorophyll; mean R^2 between 0.40 and 0.86; Figure 4). PRI was significantly correlated with Fv/Fm, RWC and the electron transport rate (ETR), and predawn PRI decreased with the minimum temperature and explained 55% of the variability for mango leaves [87].

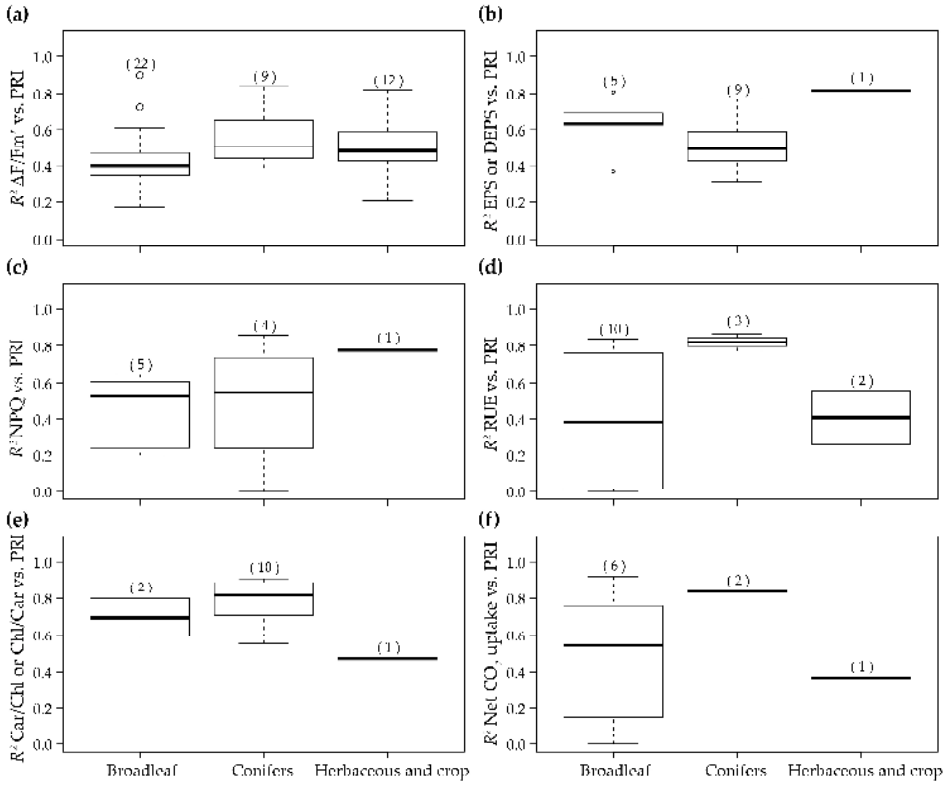

Figure 3. Boxplots of the coefficients of determination of the relationships between PRI and physiological variables at the foliar level and seasonal timescale: (**a**) Actual photochemical efficiency (ΔF/Fm'); (**b**) Epoxidation or de-epoxidation state of xanthophylls (EPS or DEPS); (**c**) Non-photochemical quenching (NPQ); (**d**) Radiation-use efficiency (RUE); (**e**) Carotenoid/chlorophyll (Car/Chl) or chlorophyll/carotenoid (Chl/Car) ratio; and (**f**) Net CO_2 uptake. Central lines represent medians, boxes represent 50% of the data, whiskers represent minima and maxima and circles represent outliers. The numbers of correlations reported in the literature are shown in brackets.

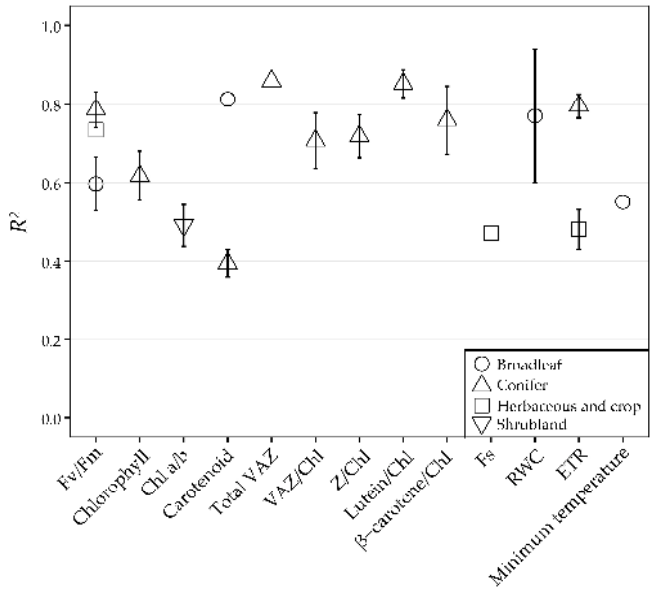

Figure 4. The mean values of coefficients of determination of the relationships between several physiological variables and PRI at the foliar level and seasonal timescale. All the correlations were significant ($p < 0.05$). Error bars indicate standard error.

3.2. Canopy Level

3.2.1. Diurnal Changes

Only 12 articles in the last two decades reported canopy PRI for tracking ecophysiological changes at short daily timescales. Ten studies published after 2010 illustrated the increasing applicability of PRI at the canopy scale. The correlations between PRI and ecophysiological variables were lower at the canopy than the foliar level. PRI explained 44%–74% of the variability of the actual quantum yield for broadleaved and herbaceous/crop plants but accounted for only 1%–40% of the variability of ΔFv/Fm' for mixed forests (Figure 5a). PRI also explained 23% and 38% of the variability of RUE for two broadleaved species under salinity stress (Figure 5d) [111]. Median R^2 between PRI and RUE and net CO_2 was as high as 0.66 and 0.63, respectively, for herbaceous/crop species (Figure 5d,f). One article reported an R^2 between PRI and the chlorophyll/carotenoid ratio of 0.65 in *Pinus sylvestris* (Figure 5e) [117]. Two articles reported that PRI correlated well with NPQ, with a median R^2 of 0.73 (Figure 5c). Three other articles reported slightly variable relationships between PRI and EPS for conifers (Figure 5b).

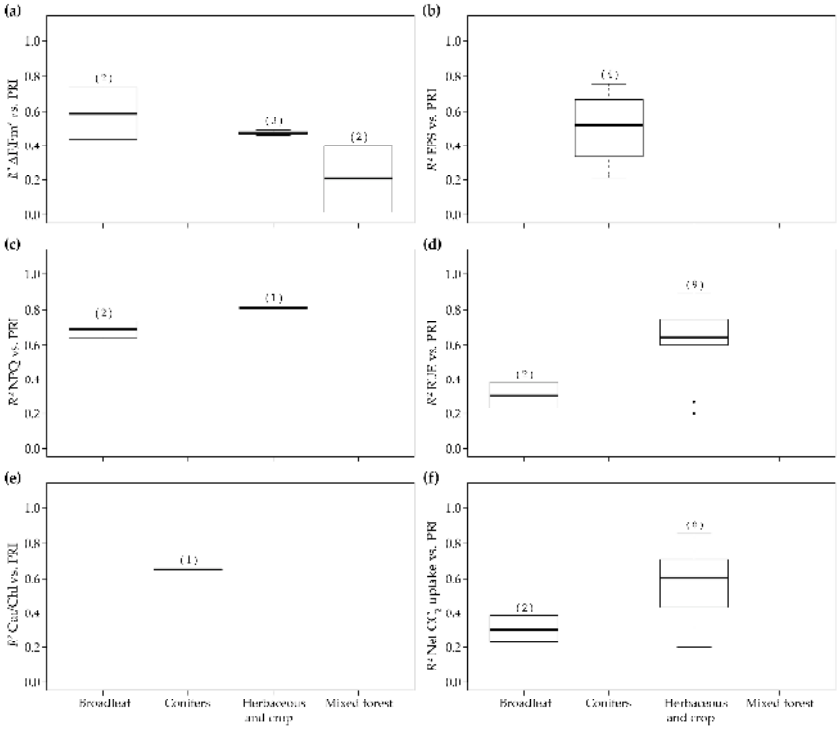

Figure 5. Boxplots of the coefficients of determination of the relationships between PRI and the physiological variables at the canopy level and diurnal timescale: (**a**) Actual photochemical efficiency (ΔF/Fm'); (**b**) Epoxidation state of xanthophylls (EPS); (**c**) Non-photochemical quenching (NPQ); (**d**) Radiation-use efficiency (RUE); (**e**) Carotenoid/chlorophyll (Car/Chl); and (**f**) Net CO_2 uptake. Central lines represent medians, boxes represent 50% of the data, whiskers represent minima and maxima and circles represent outliers. The numbers of correlations reported in the literature are shown in brackets.

Changes in PRI were significantly correlated with pigment contents, similar to the correlation at the foliar level (Figure 6). PRI was strongly correlated with Fv/Fm and non-photochemical quenching (qN) for shrubland at three sites in northern Europe but not for shrubland at southern sites due to the dominance of soil reflectance [62]. PRI explained a mean of 21%–46% and 21%–56% of the variability of water potential and stomatal conductance, respectively. The change in PPFD explained 86% of the change in diurnal PRI patterns for conifers [84], which demonstrated a strong effect of illumination on diurnal PRI patterns.

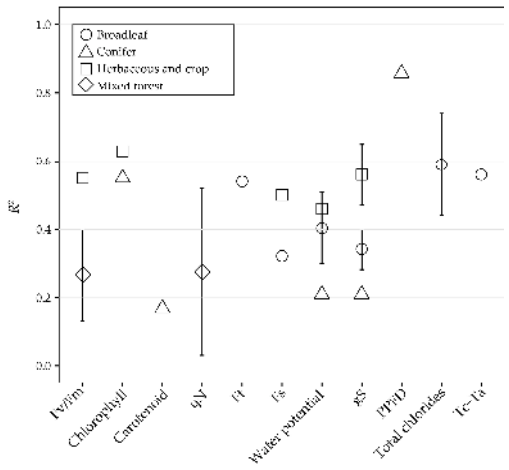

Figure 6. The mean values of coefficients of determination of the relationships between PRI and several physiological variables at the canopy level and short daily timescale. All the correlations were significant ($p < 0.05$) except for one relationship between PRI and carotenoid in *Pinus sylvestris* [117] and one between PRI and steady-state chlorophyll fluorescence (Ft) [73]. Error bars indicate standard error.

3.2.2. Seasonal Changes

Only a few studies reported correlations between PRI and ΔFv/Fm' (n = 2), EPS (n = 1) and the chlorophyll/carotenoid ratio (n = 1) at long-term (seasonal to inter-annual) timescales, with R^2 between 0.44 and 0.78 (Figure 7a–c). Twenty-four articles, however, linked seasonal or inter-annual changes in PRI with RUE at individual-plant to stand levels. Median R^2 (0.79 and 0.65, respectively; Figure 7d) was 7.0% and 4.0% higher for broadleaved and coniferous trees, respectively, than those (R^2 = 0.72 and 0.61, respectively) in Figure 5 in Garbulsky et al. [20]. PRI accounted for 66% of the variability of RUE over an entire growing season for a mixed forest [107]. Four articles published after 2010 illustrated that PRI was strongly correlated with changes in net CO_2 uptake for broadleaved (R^2 = 0.59 and 0.75) and herbaceous/crop (R^2 = 0.54 and 0.81) plants (Figure 7e).

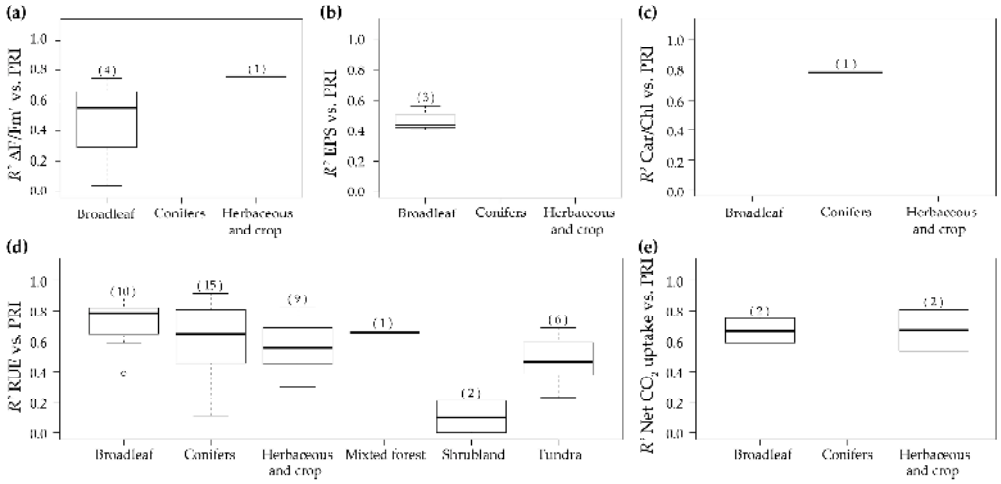

Figure 7. Boxplots of the coefficients of determination of the relationships between PRI and physiological variables at the canopy level and seasonal timescale: (**a**) Actual photochemical efficiency (ΔF/Fm'); (**b**) Epoxidation state of xanthophylls (EPS); (**c**) Carotenoid/chlorophyll ratio (Car/Chl); (**d**) Radiation-use efficiency (RUE); and (**e**) Net CO_2 uptake. Central lines represent medians, boxes represent 50% of the data, whiskers represent minima and maxima and circles represent outliers. The numbers of correlations reported in the literature are shown in brackets.

Some studies also analyzed the correlations of PRI with water content (RWC, R^2 = 0.64) [150] and stomatal conductance (gS, R^2 = 0.46) [125]. One study reported that PRI varied with the difference between foliar and air temperature for maize (R^2 = 0.82) [150]. Another study illustrated that PRI obtained from a multi-angular spectroradiometer varied with the change in the fraction of the canopy shadow (α_s) [4] under constant RUE (0.45 g CMJ^{-1}) for Douglas fir (R^2 = 0.45) and Aspen (R^2 = 0.83).

3.3. Ecosystemic Level

PRI obtained from MODIS using different reference bands was generally used for estimating ecosystemic RUE and GPP [20]. Tower or tripod-mounted spectroradiometers were also used to study ecosystemic carbon uptake at long timescales [77,123]. Forty relationships in 14 articles linked PRI with RUE based on eddy covariance in various kinds of ecosystems (e.g., Mediterranean forests, temperate deciduous forests, mountain grassland, evergreen tropical rainforest and boreal and coniferous forests; Table 1). Median R^2 for the correlations between RUE and PRI ranged from 0.12 to 0.59 (Figure 8a), with few non-significant relationships during severe drought years [25]. The correlation between PRI and RUE (R^2 = 0.12, $p < 0.001$) for a tropical evergreen forest [77] was lower than that for broadleaf (0.59 of median R^2) and coniferous forests (0.39 of median R^2), indicating a site-specific difference for the PRI-RUE relationships. PRI was significantly correlated with net CO_2 uptake for Mediterranean forests (R^2 was 0.28 [123] and 0.38 [28]; Figure 8b) and grassland ecosystems (R^2 ranged between 0.13 and 0.81 [136,153]; Figure 8b).

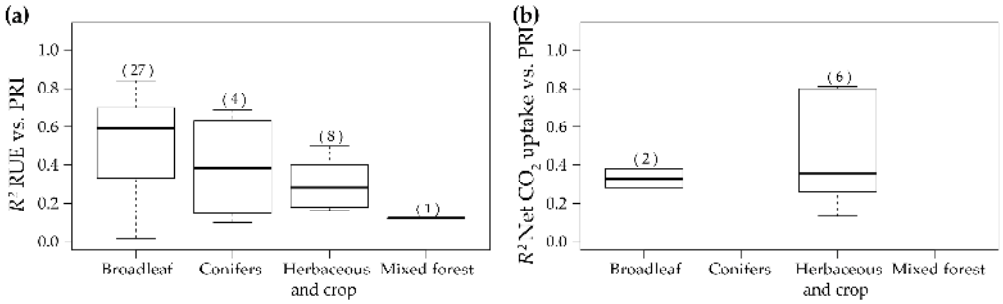

Figure 8. Boxplots of the coefficients of determination of the relationships between PRI and (**a**) Radiation-use efficiency (RUE) and (**b**) Net CO_2 uptake at the ecosystemic level and seasonal timescale. Central lines represent medians, boxes represent 50% of the data and whiskers represent minima and maxima. The numbers of correlations reported in the literature are shown in brackets.

3.4. RUE-PRI Relationships Across Scales

We calculated the mean R^2 between RUE and PRI at short daily and long seasonal scales from foliar to ecosystemic levels (Figure 9). All correlations were strong across spatiotemporal scales, with the mean R^2 ranging between 0.45 and 0.66. Mean R^2 values at daily timescales were similar to those in Figure 10 in Garbusky et al. [20] at foliar and canopy levels. The mean R^2 values at seasonal scales, however, were 20% and 7% higher for foliar and canopy levels, respectively, than those in Figure 10 in Garbusky et al. [20]. Also, the mean R^2 was higher for seasonal than diurnal relationships at the canopy scale. Forty relationships linked changes in RUE with PRI at the ecosystemic level, which was the second largest number of relationships, with a standard error of 0.04. Thirty-four of these relationships were reported after 2010. Daily PRI was thus better correlated with RUE at the foliar than the canopy level, whereas seasonal PRI tracked the changes in RUE better at the canopy than the foliar and ecosystemic levels.

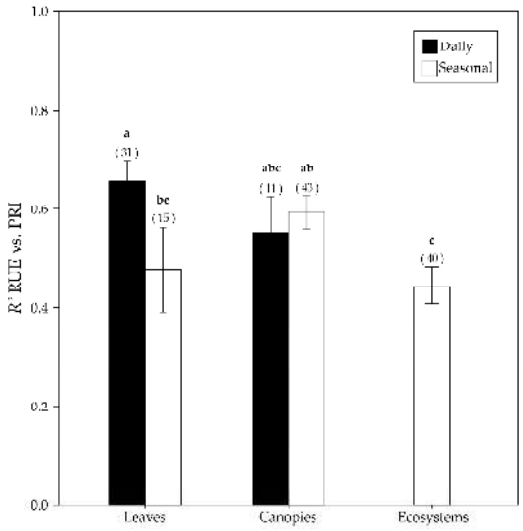

Figure 9. Comparison of the strength of the relationships between PRI and RUE across temporal and spatial scales. Each bar represents the average coefficient of determination for each source of temporal variation (daily or seasonal) and spatial scales (leaf, canopy and ecosystem). Different letters indicate significant differences ($p < 0.05$). Error bars represent the standard errors, and the numbers of reported correlations are shown in brackets.

4. Improvements in PRI Implementation

As stated above, a series of factors hinder the interpretation of PRI and its capacity to detect RUE from foliar to ecosystemic levels and at different temporal scales. The minimization and avoidance of these influences on PRI variation has thus become an urgent problem given its significance in the study of global carbon fixation. Improving the accuracy of PRI interpretation and particularly its application to long-term and global carbon uptake will require: (1) employing different kinds of instruments and models, from ground-based to space-borne satellite sensors; (2) choosing reference bands for PRI calculation (Table 2) and (3) combining other parameters and generating PRI models.

Table 2. PRI formulations for assessing RUE or net CO_2 uptake.

	Formulation	References
Original	PRI = (R531 − R570)/(R531 + R570)	Gamon et al. [18] Peñuelas et al. [19]
Different bands	PRI586 = (R531 − R586)/(R531 + R586)	Panigada et al. [148]
	PRI515 = (R531 − R515)/(R531 + R515) PRI512 = (R531 − R512)/(R531 + R512)	Calderón et al. [101] Hernández-Clemente et al. [69,117] Rossini et al. [136,150] Stagakis et al. [126] Zarco-Tejada et al. [120]
	PRI = (R525 − R570)/(R525 + R570) PRI = (R539 − R570)/(R539 + R570) PRI = (R545 − R570)/(R545 + R570) PRI = (R532 − R701)/(R532 + R701)	Stagakis et al. [60,132] Porcar-Castell et al. [72]
	PRI551 = (R531 − R551)/(R531 + R551) PRI555 = (R531 − R555)/(R531 + R555) PRI645 = (R531 − R645)/(R531 + R645) PRI667 = (R531 − R667)/(R531 + R667)	Rossini et al. [136] (simulated MODIS bands)
	PRI = (Band11 − Band1)/(Band11 + Band1) PRI = (Band11 − Band12)/(Band11 + Band12) PRI = (Band11 − Band13)/(Band11 + Band13)	Garbulsky et al. [28] (MODIS) Guarini et al. [25] (MODIS) Moreno et al. [31] (MODIS) Sims et al. [134] (MODIS) Vicca et al. [135] (MODIS)
	PRI600 = (R531 − R602)/(R531 + R602) PRI670 = (R531 − R668)/(R531 + R668)	Rossini et al. [150]

Table 2. *Cont.*

	Formulation	References
Different formulations	ΔPRI = cPRI − PRI (cPRI is dark-state PRI)	Gamon and Berry [67]
	PRIc = PRI − PRI0	Soudani et al. [123] Hmimina et al. [86,107]
	PRIs = (PRI + 1)/2	Ainsworth et al. [115] Guarini et al. [25] Rossini et al. [129] Wu et al. [109]
	$\Delta PRI = PRI_{midday} - PRI_{pre\text{-}dawn}$	Ripullone et al. [30]
	$\Delta PRI = PRI - PRI_{Ref}$ (PRI_{Ref} is the minimum PRI near midday)	Liu et al. [110]
Combination with other indices	PRInorm = PRI/(RDVI × R700/R670)	Zarco-Tejada et al. [75]
	Chlorophyll index (NDVI, NDSI, MTCI, NDI and CI)	Garrity et al. [105] Rossini et al. [129,136] Hernández-Clemente et al. [117]
	$\Delta PRI\Delta\alpha_s^{-1}$	Hall et al. [151] Hilker et al. [4,71]
	CPRI = PRI − (0.645 × ln(mNDVI705) + 0.0688)	Rahimzadeh-Bajgiran et al. [88]
	PRI_{R1} = (R550 − R531)/(R550 − R570) PRI_{R2} = (R531 − R570)/(2R550 − R531 − R570)	Wu et al. [109]
	sPRI = 0.15 × (1 − exp (−0.5 × LAI)) − 0.2 rPRI = PRI − sPRI	Wu et al. [124]
	SIF	Cheng et al. [81] Rossini et al. [129]
	VPD	Nakaji et al. [77]
	fAPAR estimated as MTCI	Rossini et al. [136] (MODIS)
	PRIn = PRI − PRI0 sPRIn = (1 + PRIn)/2	Vicca et al. [135] (MODIS)

4.1. Instruments

Various instruments have been used for obtaining PRI in addition to the traditional ground-based spectroradiometer. A PRI imaging system was developed using a low-cost CCD camera and band-pass filters (530 and 570 nm) to non-destructively evaluate micropropagated plantlets, and has been successfully tested in cultured plantlets and from outside the culture vessels [89,140]. An automated multi-angular spectroradiometer (AMSPEC I and II system) [4] was designed and CHRIS/PROBA was used [71,90,151,154] for instantaneously measuring the spectra of a canopy at multiple detection angles along the tracking path, and for illustrating the effect of canopy structure and detection geometry at various spatial scales. CHRIS/PROBA, however, can only provide a very limited spatial coverage, which inhibits the monitoring of multiple-angular PRI at regional and global scales [154]. A temperature-controlled spectrometric system was also designed to collect high resolution spectral data to detect the diurnal and seasonal variation of RUE and fluorescence [137]. Other instruments, such as a simple filtered photodiode (QuadPod) [155], a low-cost spectroscopic instrumentation (PRiAnalyze) [130] and an automated PRI sensor with upward- and downward-facing sensors [76], were developed to explore the environmental and physiological constraints on photosynthesis and to improve remote-sensing studies of carbon uptake.

4.2. Modeling

Models of radiative transfer have been applied to explore the changes in PRI influenced by a variety of detection geometries, illumination conditions and canopy structures in conjunction with in situ measurements [4,31,69,75,82,83,109,117,128,133,151,154]. The accuracy of the simulated PRI from ACRM (A Markov chain Analytical two-layer Canopy Reflectance Model) was affected by

canopy structural change and thus led to inaccurate estimates of RUE and GPP [83]. Empirical regression models were effectively used to assess PRI and ecophysiological variation [87,109,113,124]. Devising a valid model is therefore important for accurately estimating PRI and providing a continuous assessment of GPP.

4.3. Different Formulations of PRI

The application of the xanthophyllic cycle and different reference bands has been discussed extensively for better understanding PRI (Table 2). Porcar-Castell et al. [72] used PRI calculated as (R545 − R570)/(R545 + R570), which has been associated with the rapidly conformational changes contributing to protonation in key proteins in the thylakoid membrane during reversible NPQ and has improved the correlations between NPQ and PRI, especially during early spring decoupling in conifers. A combination of a vegetation index of the xanthophyllic de-epoxidation band (531 nm) with a band associated with chlorophyllic content (701 nm from CHRIS) performed better than PRI for estimating seasonal RUE from the backscatter direction [60]. PRI515 (or PRI512) has recently been proposed to minimize the effects of canopy structure under different stresses [69,101,117,120,126] but was not significantly correlated with GPP for an olive orchard [149] and performed slightly weaker than PRI for crops under water stress [148,150]. Panigada et al. [148] reported that PRI570 and PRI586 correlated with ΔF/Fm′ (R^2 = 0.49 and 0.51, respectively) for cereal crops under water stress better than other PRIs based on different reference wavelengths. Additionally, PRIs based on green reference bands at 555 and 551 nm correlated mostly with RUE, and PRIs based on reference bands at 645 and 667 nm correlated better with the leaf chlorophyllic concentration than with RUE [136].

The first derivative of PRI with respect to shadow fractions viewed by the sensor ($\Delta PRI \Delta \alpha_s{}^{-1}$ or PRI′) was developed to alleviate the impacts of vegetation structure and radiometric properties on the basis of a multi-angular observation algorithm, which has been used to infer RUE across different biomes [4,71,151,154]. The proposed PRI′ technique, however, was probably not applicable to infer RUE for canopies with reduced variability in shadow fractions as noted by Hilker et al. [71]. Gamon and Berry [67] showed that a combination of dark-state sampling (cPRI) and dark-to-light conversion (ΔPRI) could experimentally isolate the two (constitutive and facultative) effects on PRI in situ without extensive destructive sampling, which could help to interpret the variation in the PRI signal from remote platforms. Differences in canopy PRI (ΔPRI) from the minimum reference PRI near midday [110] were similarly applied and improved the correlations between RUE and PRI (R^2 = 0.24 for PRI and 0.5 for ΔPRI). Differences in foliar PRI (ΔPRI, dawn PRI minus midday PRI) [30] improved the correlation with the maximum photosynthetic rate (R^2 = 0.21 for PRI and 0.44 for ΔPRI). Some studies also reported the use of scaled PRI (sPRI = (PRI + 1)/2) to avoid negative values and for comparable analysis [25,115,129,135].

A corrected PRI (PRIc = PRI − PRI0), after subtracting an estimated PRI0 defined as PRI of perfectly dark-adapted leaves, correlated well with RUE at diurnal [86], seasonal [86,123] and inter-annual scales [123]. This approach considered the impacts of changes in canopy structure and pigments, which greatly improved the correlations between PRI and RUE (Figure 10a) with a increment of R^2 by 71% and 92% at the foliar level in oak and beech, respectively [86], and by 22% for a deciduous broadleaved forest [123]. The correlation between PRI and RUE, however, was not improved by correcting with PRI0 for an evergreen forest, because PRI0 varied little across the season [123]. Hmimina et al. [107] developed an accurate deconvolution model for further improving PRI0 and PRIc to identify the influences of pigment and physiological changes on PRI variation and improved the correlation with RUE from an exponential correlation of 0.66 to a highly significant linear correlation of 0.93. Vicca et al. [135] similarly applied PRIc (method from Soudani et al. [123]) using MODIS data, successfully removed the impact of pigment and illumination and detected the severe drought and GPP variation for a deciduous broadleaved forest that was not detected by EVI. Wu et al. [109] also revised PRI by introducing the optical signal of chlorophyllic content at 550 nm to decrease the effect of the sizes of pigment pools; two revised

indices, PRI_{R1} = (R550 − R531)/(R550 − R570) and PRI_{R2} = (R531 − R570)/(2R550 − R531 − R570), correlated better with RUE, particularly during senescence when chlorophyllic content and LAI were low (R^2 = 0.57 and 0.59 for PRI_{R1} and PRI_{R2}, respectively; R^2 = 0.20 for PRI). The residual PRI (rPRI = PRI − sPRI), which removed the structural-related signal in PRI (sPRI) as a function of LAI, increased by 42% the correlation in the estimation of RUE over PRI [124]. In other studies, the calibrated PRI (CPRI = PRI – (0.645 × ln(mNDVI705) + 0.0688)) adjusted the effects of the pigments and improved the correlation between PRI and NPQ [88]. PRI calculated as PRInorm = PRI/(RDVI × R700/R670) (RDVI, Renormalized Difference Vegetation Index [156]) which normalizes for decreases in chlorophyllic content and canopy leaf area induced by stress was better correlated with stomatal conductance, water potential and pigment content and detected water stress better than the standard PRI [75].

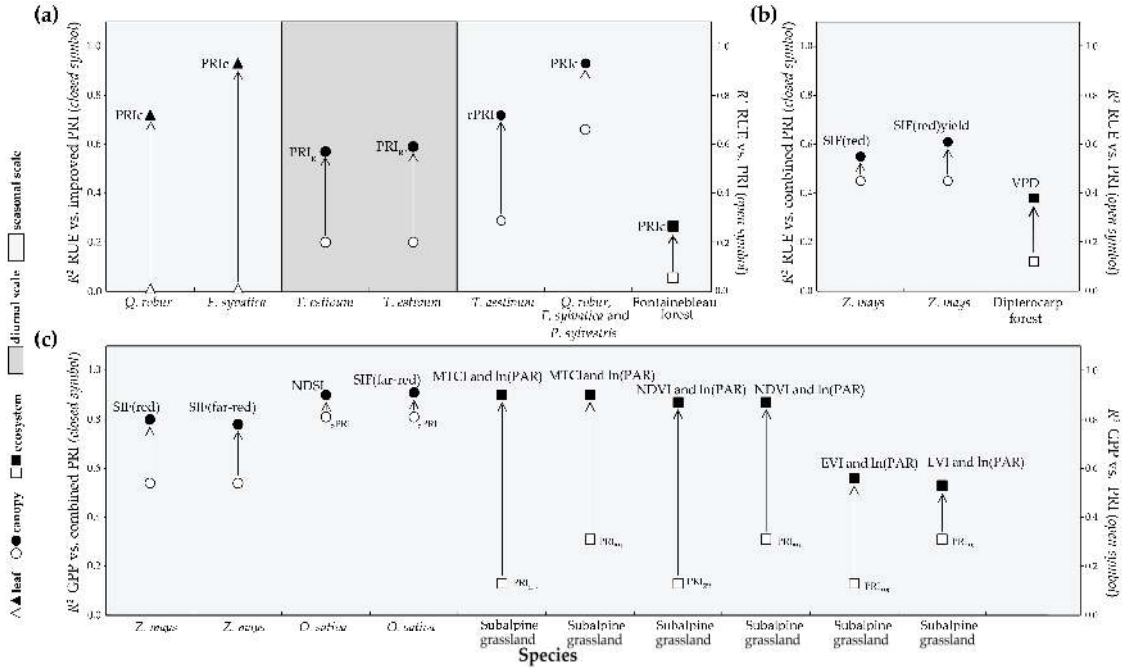

Figure 10. Comparison of the relationships between RUE/GPP vs. PRI and RUE/GPP vs. improved/combined PRI. (**a**) PRIc was used for *Q. robur* and *F. sylvatica* [86], a mixed canopy of *Q. robur*, *F. sylvatica* and *P. sylvestris* [107] and a deciduous broadleaved forest [123]; PRI_{R1} and PRI_{R2} were used for *T. aestivum* [109] and rPRI for *T. aestivum* (mixed non-linear model, rPRI = PRI − (0.15 × (1 − exp(−0.5 × LAI)) − 0.2)) [124]; (**b**) Tracking RUE combining PRI with SIF (red) or SIF (far-red) yield in *Z. mays* (RUE = a + b × PRI + c × SIF + d × PRI × SIF) [81] and with VPD in a dipterocarp forest (RUE = 0.153 × PRI − 0.00067 × VPD + 0.029) [77]; (**c**) Tracking GPP combining PRI with SIF (red) or SIF (far-red) in *Z. mays* (GPP = a + b × PRI + c × SIF + d × PRI × SIF) [81], with NDSI (GPP = (a0 × sPRI + a1) × (a2 × NDSI + a3) × PARi, sPRI = (1 + PRI)/2) and SIF (far-red, GPP = (a0 × sPRI + a1) × (a2 × SIF + a3), sPRI = (1 + PRI)/2) in *O. sativa* [129] and with VI (MTCI, NDVI and EVI) and ln(PAR) (GPP = (a0 × PRI + b0) × (a × VI + b) × ln(PAR)) [136] in a subalpine grassland.

4.4. Combining with Other Parameters to Evaluate Carbon Fixation

Combining PRI with other vegetation indices (VIs) was a promising approach in the review by Garbulsky et al. [20] to improve the detection of carbon uptake. The conventional and widely used RUE model expresses GPP as the product of APAR and RUE. PRI is a proxy of RUE, so some VIs (e.g., normalized difference spectral indices (NDSI), NDVI, the MERIS terrestrial chlorophyll index (MTCI) and EVI) correlate well with the fraction of APAR (fAPAR) [10,14–17,20,24,129,136]. GPP can thus be efficiently assessed with the combination of MODIS VIs and PRI, and the correlations were

22%–77% higher than with PRI (Figure 10c) [136]. Estimation of seasonal GPP based on MTCI-related fAPAR and PRI-related RUE (PRI551, MODIS band 4 as the reference band) modeled a subalpine grassland best (R^2 = 0.90) [136].

SIF, another photoprotective mechanism successfully sensed from space, is also an indicator of vegetation function and is used for carbon modeling [157,158]. The combination of SIF with PRI is strongly correlated with RUE and GPP for crops (Figure 10b,c). Combining PRI and SIF in a linear regression model improved GPP estimation for a cornfield (R^2 = 0.8 for SIF at red band and 0.78 for SIF at far-red band, Figure 10c) [81]. Gross ecosystemic productivity (GEP) for a rice crop was best estimated based on APAR as a function of steady-state SIF computed at 760 nm (SIF(far-red)) and on RUE as a function of sPRI (Figure 10c) [129], which was the first study that modeled seasonal courses of GEP based on measurements of remotely sensing fluorescence. Nakaji et al. [77] demonstrated that the accuracy of estimating RUE (Figure 10b) and the estimation error were improved for an evergreen tropical rainforest by applying a regression model using PRI and VPD, probably due to the influence of the water conditions on unseasonal variation in RUE.

5. Discussion

The factors affecting PRI variation at different spatiotemporal scales were reviewed in this study based on the most recent publications in which PRI has received increasing attention and on the previous publications reviewed by Garbulsky et al. [20]. Our more than 20 years' analysis shows that diurnal changes in PRI were strongly correlated with EPS at both the foliar and canopy levels (Figures 1 and 5) across more vegetation species than those reported in the first study reviewed by Garbulsky et al. [20]. Interestingly, the relationships of seasonal PRI with Chl/Car ratios were stronger than with EPS at both foliar and canopy levels for different species (Figures 1 and 3). Such results indicate the significant impacts of xanthophyll-cycle pigments on short-term changes of PRI, and chlorophyll and carotenoid pool sizes on long-term changes of PRI, in accordance with the reported studies by Wong and Gamon [54,55]. Our analysis thus further supports that taking into account the changes in chlorophyll and carotenoid pool sizes is critical for PRI interpretation on long timescales. Our summarized correlations between PRI and ecophysiological variables linked to RUE (Figures 1–8) show that PRI is a good proxy of photosynthetic efficiency at foliar, canopy and ecosystemic levels. The mean R^2 values between PRI and RUE at diurnal and seasonal scales from foliar to ecosystemic levels in this study (Figure 9) were even higher than in the first study reviewed by Garbulsky et al. [20]. Further, the significant relationships of PRI with water status (relative water content (RWC) and water potential) suggest that PRI also could be appropriate for water stress assessment.

Nevertheless, the factors complicating PRI interpretation still hinder the use of generalized PRI-RUE relationships. Our summarized review of improvements in PRI implementation found, however, that key factors driving PRI variation, such as the sizes of pigment pools and canopy structure could be minimized or avoided in part to make PRI an efficient indicator of RUE. Such improvement could be possible through subtracting the dark-adapted PRI and introducing the optical signal of pigment pools or the structural-related signal. Moreover, our analysis also showed that combining RUE-related PRI with APAR-related greenness biomass indices (e.g., NDVI, MTCI and EVI; Table 2) efficiently explores GPP (Figure 10), as expected in the previous review by Garbulsky et al. [20]. On the other hand, most reported publications focused on broadleaf and herbaceous and crops during last two decades (Table 1), so expanding the study to a wide range of plant functional types is necessary.

The strong correlations of PRI with actual photochemical efficiency, especially with RUE and net CO_2 uptake across different plant functional types and spatiotemporal scales, indicate the possibility of assessing photosynthetic activity at larger scales. Besides, MODIS PRI has been increasingly and successfully used to assess ecosystemic RUE, allowing us to expect a PRI product in platforms such as the commonly used NDVI.

6. Conclusions and Perspectives

The mechanisms involved in PRI variation can be complex due to varying spatial and temporal scales. Many physical, biochemical and physiological factors can affect diurnal and seasonal PRI patterns at foliar, canopy and ecosystemic levels. Most of the variation of PRI when scaling up from diurnal to seasonal measurements is likely due to the changes in the size of the constitutive pigment pools other than facultative xanthophyllic de-epoxidation [54,55,67]. Other physical or external factors, such as illumination, temperature or water stress, soil background, disease and low nitrogen levels, have the potential to produce biochemical and physiological changes that can also generate PRI variation. The structural properties of canopies and the solar/spectrometric (or satellite) directions of detection at the canopy and ecosystemic levels are also important factors that contribute to changes in PRI. Our analysis, however, also indicated that PRI was often significantly correlated with ecophysiological variables and RUE. R^2 values between PRI and RUE ranged between 0.41 and 0.66 (Figure 9), even higher than in the first studies reviewed by Garbulsky et al. [20]. In particular, PRI was a good indicator of diurnal changes in RUE and a good proxy of seasonal changes in photosynthetic efficiency at different spatial scales.

Our understanding of the ecophysiological mechanisms of PRI variation and the implementation of PRI, particularly for assessing carbon uptake, have progressed. Further, other photoprotective mechanisms, for example chloroplast avoidance movement, have been proposed to have an effect on light-induced optical changes related to zeaxanthin formation [159] that probably also play a role in the PRI variation. Such influences on PRI variation should be further analyzed. The correlations between PRI and RUE have been greatly improved by decreasing the impact of the canopy structure and the sizes of the pigment pools. These impacts can be decreased by subtracting the dark-adapted PRI to minimize the influence of the canopy structure and the pigment pools and by introducing the optical signal of the pigment pools or the structural-related signal. GPP, though, can be better assessed by combining the RUE-related PRI with APAR-related greenness indices, thus using the approach of the RUE model. Combining SIF with PRI is another promising opportunity for interpreting RUE and monitoring GPP from local to regional scales.

Studies of the optical remote sensing of RUE, especially using PRI to estimate or model RUE, have focused mainly on temperate forests and grassland, with limited studies of tropical forests. More attention should thus be paid to the assessment of RUE and GPP using PRI for different species, especially for tropical forests. We should also further explore the PRI mechanisms across vegetation types and at various spatial and temporal scales. Unmanned aerial vehicles (UAVs) with various multispectral cameras can increasingly provide an exciting opportunity to obtain canopy PRI and also SIF with high spatiotemporal resolution [74,75,149,160], which could be very beneficial for our understanding of the variation in canopy PRI. Our results indicate that corrected PRI (PRIc) proposed by Soudani et al. [123] is an outstanding improved PRI, which could be a promising proxy of RUE and is warranted to be tested over a wide range of species and spatiotemporal scales. Furthermore, PRIc was successfully obtained from MODIS and tracked the severe drought episode and GPP variation. Thus, we advocate efforts to produce a PRI product in platforms (e.g., MODIS PRI) as existing MODIS NDVI/EVI products. Additionally, PRI coupled with SIF or indices of greenness biomass is a promising approach to build an integrated and robust model of remotely sensed carbon uptake. We can attempt to combine PRI corrected or calibrated by the most influential factors (e.g., pigment pool sizes and structural changes) with SIF or other greenness indices to establish a generalized global model of carbon uptake. The satellite data from MODIS and GOME (Global Ozone Monitoring Experiment) provide potential regional and global calculations of PRI. The Sentinel program [161] of the ESA (European Space Agency), the new hyperspectral instruments built by the DLR (German Aerospace Center), such as EnMAP (Environmental Mapping and Analysis Program [162]) or DESIS (Earth Sensing Imaging Spectrometer [163]) on board the ISS (International Space Station), as well as the forthcoming missions built by NASA (National Aeronautics and Space Administration), such as the HyspIRI (Hyperspectral Infrared Imager [164]) or the EIS (Europa Imaging System [165]) allow space-based calculation of the

PRI and estimation of the RUE at a higher spatial resolution. Incorporating satellite data with over 685 eddy covariance flux sites (FLUXNET [166]) even further enhances the global continuous and accurate monitoring of carbon uptake by terrestrial ecosystems.

Acknowledgments: This research was supported by the European Research Council Synergy grant SyG-2013-610028 IMBALANCE-P, the Spanish Government project CGL2013-48074-P and the Catalan Government project SGR 2014-274. Chao Zhang gratefully acknowledges the support from the China Scholarship Council.

Author Contributions: Iolanda Filella, Josep Peñuelas and Chao Zhang planned and designed the research. Martin F. Garbulsky provided data from 1992 to 2009. Chao Zhang wrote the main manuscript text and prepared the figures and tables. All authors contributed significantly to the final revisions of the manuscript.

Conflicts of Interest: The authors declare no conflict of interest.

References

1. Beer, C.; Reichstein, M.; Tomelleri, E.; Ciais, P.; Jung, M.; Carvalhais, N.; Rödenbeck, C.; Arain, M.A.; Baldocchi, D.; Bonan, G.B.; et al. Terrestrial gross carbon dioxide uptake: Global distribution and covariation with climate. *Science* **2010**, *329*, 834–838. [CrossRef] [PubMed]
2. Schimel, D.; Pavlick, R.; Fisher, J.B.; Asner, G.P.; Saatchi, S.; Townsend, P.; Miller, C.; Frankenberg, C.; Hibbard, K.; Cox, P. Observing terrestrial ecosystems and the carbon cycle from space. *Glob. Chang. Biol.* **2015**, *21*, 1762–1776. [CrossRef] [PubMed]
3. Guanter, L.; Zhang, Y.; Jung, M.; Joiner, J.; Voigt, M.; Berry, J.A.; Frankenberg, C.; Huete, A.R.; Zarco-Tejada, P.; Lee, J.-E.; et al. Global and time-resolved monitoring of crop photosynthesis with chlorophyll fluorescence. *Proc. Natl. Acad. Sci. USA* **2014**, *111*, E1327–E1333. [CrossRef] [PubMed]
4. Hilker, T.; Hall, F.G.; Coops, N.C.; Lyapustin, A.; Wang, Y.; Nesic, Z.; Grant, N.; Black, T.A.; Wulder, M.A.; Kljun, N.; et al. Remote sensing of photosynthetic light-use efficiency across two forested biomes: Spatial scaling. *Remote Sens. Environ.* **2010**, *114*, 2863–2874. [CrossRef]
5. Joiner, J.; Yoshida, Y.; Vasilkov, A.P.; Schaefer, K.; Jung, M.; Guanter, L.; Zhang, Y.; Garrity, S.; Middleton, E.M.; Huemmrich, K.F.; et al. The seasonal cycle of satellite chlorophyll fluorescence observations and its relationship to vegetation phenology and ecosystem atmosphere carbon exchange. *Remote Sens. Environ.* **2014**, *152*, 375–391. [CrossRef]
6. Mäkelä, A.; Pulkkinen, M.; Kolari, P.; Lagergren, F.; Berbigier, P.; Lindroth, A.; Loustau, D.; Nikinmaa, E.; Vesala, T.; Hari, P. Developing an empirical model of stand GPP with the LUE approach: Analysis of eddy covariance data at five contrasting conifer sites in Europe. *Glob. Chang. Biol.* **2008**, *14*, 92–108. [CrossRef]
7. Piao, S.; Sitch, S.; Ciais, P.; Friedlingstein, P.; Peylin, P.; Wang, X.; Ahlström, A.; Anav, A.; Canadell, J.G.; Cong, N.; et al. Evaluation of terrestrial carbon cycle models for their response to climate variability and to CO_2 trends. *Glob. Chang. Biol.* **2013**, *19*, 2117–2132. [CrossRef] [PubMed]
8. Gamon, J.A. Reviews and syntheses: Optical sampling of the flux tower footprint. *Biogeosciences* **2015**, *12*, 4509–4523. [CrossRef]
9. Garbulsky, M.F.; Filella, I.; Verger, A.; Peñuelas, J. Photosynthetic light use efficiency from satellite sensors: From global to Mediterranean vegetation. *Environ. Exp. Bot.* **2014**, *103*, 3–11. [CrossRef]
10. Hilker, T.; Coops, N.C.; Wulder, M.A.; Black, T.A.; Guy, R.D. The use of remote sensing in light use efficiency based models of gross primary production: A review of current status and future requirements. *Sci. Total Environ.* **2008**, *404*, 411–423. [CrossRef] [PubMed]
11. Peñuelas, J.; Garbulsky, M.F.; Filella, I. Photochemical reflectance index (PRI) and remote sensing of plant CO_2 uptake. *New Phytol.* **2011**, *191*, 596–599. [CrossRef] [PubMed]
12. Monteith, J.L. Solar radition and productivity in tropical ecosystems. *J. Appl. Ecol.* **1972**, *9*, 747–766. [CrossRef]
13. Monteith, J.L. Climate and the efficiency of crop production in Britain. *Philos. Trans. R. Soc. London B Biol. Sci.* **1977**, *281*, 277–294. [CrossRef]
14. Balzarolo, M.; Vicca, S.; Nguy-Robertson, A.L.; Bonal, D.; Elbers, J.A.; Fu, Y.H.; Grünwald, T.; Horemans, J.A.; Papale, D.; Peñuelas, J.; et al. Matching the phenology of net ecosystem exchange and vegetation indices estimated with MODIS and FLUXNET *in-situ* observations. *Remote Sens. Environ.* **2016**, *174*, 290–300. [CrossRef]

15. Baret, F.; Guyot, G. Potentials and limits of vegetation indices for LAI and APAR assessment. *Remote Sens. Environ.* **1991**, *35*, 161–173. [CrossRef]
16. Rouse, J.W., Jr.; Haas, R.H.; Schell, J.A.; Deering, D.W. *Monitoring Vegetation Systems in the Great Plains with ERTS*; Freden, S.C., Mercanti, E.P., Becker, M.A., Eds.; NASA: Washington, D.C., USA, 1974; Volume 1, pp. 309–317.
17. Running, S.W.; Nemani, R.R.; Heinsch, F.A.; Zhao, M.; Reeves, M.; Hashimoto, H. A continuous satellite-derived measure of global terrestrial primary production. *Bioscience* **2004**, *54*, 547–560. [CrossRef]
18. Gamon, J.A.; Peñuelas, J.; Field, C.B. A narrow-waveband spectral index that tracks diurnal changes in photosynthetic efficiency. *Remote Sens. Environ.* **1992**, *44*, 35–44. [CrossRef]
19. Peñuelas, J.; Filella, I.; Gamon, J.A. Assessment of photosynthetic radiation-use efficiency with spectral reflectance. *New Phytol.* **1995**, *131*, 291–296. [CrossRef]
20. Garbulsky, M.F.; Peñuelas, J.; Gamon, J.A.; Inoue, Y.; Filella, I. The photochemical reflectance index (PRI) and the remote sensing of leaf, canopy and ecosystem radiation use efficiencies: A review and meta-analysis. *Remote Sens. Environ.* **2011**, *115*, 281–297. [CrossRef]
21. Gamon, J.A.; Field, C.B.; Bilger, W.; Björkman, O.; Fredeen, A.L.; Peñuelas, J. Remote sensing of the xanthophyll cycle and chlorophyll fluorescence in sunflower leaves and canopies. *Oecologia* **1990**, *85*, 1–7. [CrossRef]
22. Filella, I.; Peñuelas, J.; Llorens, L.; Estiarte, M. Reflectance assessment of seasonal and annual changes in biomass and CO_2 uptake of a Mediterranean shrubland submitted to experimental warming and drought. *Remote Sens. Environ.* **2004**, *90*, 308–318. [CrossRef]
23. Filella, I.; Porcar-Castell, A.; Munné-Bosch, S.; Bäck, J.; Garbulsky, M.F.; Peñuelas, J. PRI assessment of long-term changes in carotenoids/chlorophyll ratio and short-term changes in de-epoxidation state of the xanthophyll cycle. *Int. J. Remote Sens.* **2009**, *30*, 4443–4455. [CrossRef]
24. Coops, N.C.; Hilker, T.; Hall, F.G.; Nichol, C.J.; Drolet, G.G. Estimation of light-use efficiency of terrestrial ecosystems from space: A status report. *Bioscience* **2010**, *60*, 788–797. [CrossRef]
25. Guarini, R.; Nichol, C.; Clement, R.; Loizzo, R.; Grace, J.; Borghetti, M. The utility of MODIS-sPRI for investigating the photosynthetic light-use efficiency in a Mediterranean deciduous forest. *Int. J. Remote Sens.* **2014**, *35*, 6157–6172. [CrossRef]
26. Nichol, C.J.; Huemmrich, K.F.; Black, T.A.; Jarvis, P.G.; Walthall, C.L.; Grace, J.; Hall, F.G. Remote sensing of photosynthetic-light-use efficiency of boreal forest. *Agric. For. Meteorol.* **2000**, *101*, 131–142. [CrossRef]
27. Peñuelas, J.; Inoue, Y. Reflectance assessment of canopy CO_2 uptake. *Int. J. Remote Sens.* **2000**, *21*, 3353–3356.
28. Garbulsky, M.F.; Peñuelas, J.; Ogaya, R.; Filella, I. Leaf and stand-level carbon uptake of a Mediterranean forest estimated using the satellite-derived reflectance indices EVI and PRI. *Int. J. Remote Sens.* **2013**, *34*, 1282–1296. [CrossRef]
29. Garbulsky, M.F.; Peñuelas, J.; Papale, D.; Filella, I. Remote estimation of carbon dioxide uptake by a Mediterranean forest. *Glob. Chang. Biol.* **2008**, *14*, 2860–2867. [CrossRef]
30. Ripullone, F.; Rivelli, A.R.; Baraldi, R.; Guarini, R.; Guerrieri, R.; Magnani, F.; Peñuelas, J.; Raddi, S.; Borghetti, M. Effectiveness of the photochemical reflectance index to track photosynthetic activity over a range of forest tree species and plant water statuses. *Funct. Plant Biol.* **2011**, *38*, 177–186. [CrossRef]
31. Moreno, A.; Maselli, F.; Gilabert, M.A.; Chiesi, M.; Martínez, B.; Seufert, G. Assessment of MODIS imagery to track light-use efficiency in a water-limited Mediterranean pine forest. *Remote Sens. Environ.* **2012**, *123*, 359–367. [CrossRef]
32. Evain, S.; Flexas, J.; Moya, I. A new instrument for passive remote sensing: 2. Measurement of leaf and canopy reflectance changes at 531 nm and their relationship with photosynthesis and chlorophyll fluorescence. *Remote Sens. Environ.* **2004**, *91*, 175–185. [CrossRef]
33. Filella, I.; Amaro, T.; Araus, J.L.; Peñuelas, J. Relationship between photosynthetic radiation-use efficiency of barley canopies and the photochemical reflectance index (PRI). *Physiol. Plant.* **1996**, *96*, 211–216. [CrossRef]
34. Gamon, J.A.; Serrano, L.; Surfus, J.S. The photochemical reflectance index: An optical indicator of photosynthetic radiation use efficiency across species, functional types, and nutrient levels. *Oecologia* **1997**, *112*, 492–501. [CrossRef]
35. Guo, J.; Trotter, C.M. Estimating photosynthetic light-use efficiency using the photochemical reflectance index: Variations among species. *Funct. Plant Biol.* **2004**, *31*, 255–265. [CrossRef]

36. Meroni, M.; Rossini, M.; Picchi, V.; Panigada, C.; Cogliati, S.; Nali, C.; Colombo, R. Assessing steady-state fluorescence and PRI from hyperspectral proximal sensing as early indicators of plant stress: The case of ozone exposure. *Sensors* **2008**, *8*, 1740–1754. [CrossRef]
37. Meroni, M.; Picchi, V.; Rossini, M.; Cogliati, S.; Panigada, C.; Nali, C.; Lorenzini, G.; Colombo, R. Leaf level early assessment of ozone injuries by passive fluorescence and photochemical reflectance index. *Int. J. Remote Sens.* **2008**, *29*, 5409–5422. [CrossRef]
38. Middleton, E.M.; Cheng, Y.B.; Hilker, T.; Black, T.A.; Krishnan, P.; Coops, N.C.; Huemmrich, K.F. Linking foliage spectral responses to canopy-level ecosystem photosynthetic light-use efficiency at a Douglas-fir forest in Canada. *Can. J. Remote Sens.* **2009**, *35*, 166–188. [CrossRef]
39. Nakaji, T.; Ide, R.; Takagi, K.; Kosugi, Y.; Ohkubo, S.; Nasahara, K.N.; Saigusa, N.; Oguma, H. Utility of spectral vegetation indices for estimation of light conversion efficiency in coniferous forests in Japan. *Agric. For. Meteorol.* **2008**, *148*, 776–787. [CrossRef]
40. Peguero-Pina, J.J.; Morales, F.; Flexas, J.; Gil-Pelegrín, E.; Moya, I. Photochemistry, remotely sensed physiological reflectance index and de-epoxidation state of the xanthophyll cycle in *Quercus coccifera* under intense drought. *Oecologia* **2008**, *156*, 1–11. [CrossRef] [PubMed]
41. Peñuelas, J.; Llusia, J.; Pinol, J.; Filella, I. Photochemical reflectance index and leaf photosynthetic radiation-use-efficiency assessment in Mediterranean trees. *Int. J. Remote Sens.* **1997**, *18*, 2863–2868. [CrossRef]
42. Sims, D.A.; Gamon, J.A. Relationship between leaf pigment content and spectral reflectance across a wide range species, leaf structures and development stages. *Remote Sens. Environ.* **2002**, *81*, 337–354. [CrossRef]
43. Sims, D.A.; Luo, H.; Hastings, S.; Oechel, W.C.; Rahman, A.F.; Gamon, J.A. Parallel adjustments in vegetation greenness and ecosystem CO_2 exchange in response to drought in a southern California chaparral ecosystem. *Remote Sens. Environ.* **2006**, *103*, 289–303. [CrossRef]
44. Strachan, I.B.; Pattey, E.; Boisvert, J.B. Impact of nitrogen and environmental conditions on corn as detected by hyperspectral reflectance. *Remote Sens. Environ.* **2002**, *80*, 213–224. [CrossRef]
45. Weng, J.H.; Jhaung, L.H.; Jiang, J.Y.; Lai, G.M.; Liao, T.S. Down-regulation of photosystem 2 efficiency and spectral reflectance in mango leaves under very low irradiance and varied chilling treatments. *Photosynthetica* **2006**, *44*, 248–254. [CrossRef]
46. Weng, J.H.; Chen, Y.N.; Liao, T.S. Relationships between chlorophyll fluorescence parameters and photochemical reflectance index of tree species adapted to different temperature regimes. *Funct. Plant Biol.* **2006**, *33*, 241–246. [CrossRef]
47. Peñuelas, J.; Filella, I.; Gamon, J.A.; Field, C.B. Assessing photosynthetic radiation-use efficiency of emergent aquatic vegetation from spectral reflectance. *Aquat. Bot.* **1997**, *58*, 307–315. [CrossRef]
48. Lovelock, C.E.; Robinson, S.A. Surface reflectance properties of antarctic moss and their relationship to plant species, pigment composition and photosynthetic function. *Plant Cell Environ.* **2002**, *25*, 1239–1250. [CrossRef]
49. Yamano, H.; Chen, J.; Zhang, Y.; Tamura, M. Relating photosynthesis of biological soil crusts with reflectance: Preliminary assessment based on a hydration experiment. *Int. J. Remote Sens.* **2006**, *27*, 5393–5399. [CrossRef]
50. Van Gaalen, K.E.; Flanagan, L.B.; Peddle, D.R. Photosynthesis, chlorophyll fluorescence and spectral reflectance in *Sphagnum* moss at varying water contents. *Oecologia* **2007**, *153*, 19–28. [CrossRef] [PubMed]
51. Jupa, R.; Hájek, J.; Hazdrová, J.; Barták, M. Interspecific differences in photosynthetic efficiency and spectral reflectance in two *Umbilicaria* species from Svalbard during controlled desiccation. *Czech Polar Rep.* **2012**, *40*, 31–41. [CrossRef]
52. Louis, J.; Ounis, A.; Ducruet, J.M.; Evain, S.; Laurila, T.; Thum, T.; Aurela, M.; Wingsle, G.; Alonso, L.; Pedros, R.; et al. Remote sensing of sunlight-induced chlorophyll fluorescence and reflectance of Scots pine in the boreal forest during spring recovery. *Remote Sens. Environ.* **2005**, *96*, 37–48. [CrossRef]
53. Nichol, C.J.; Lloyd, J.; Shibistova, O.; Arneth, A.; Röser, C.; Knohl, A.; Matsubara, S.; Grace, J. Remote sensing of photosynthetic-light-use efficiency of a Siberian boreal forest. *Tellus B* **2002**, *54*, 677–687. [CrossRef]
54. Wong, C.Y.S.; Gamon, J.A. The photochemical reflectance index provides an optical indicator of spring photosynthetic activation in evergreen conifers. *New Phytol.* **2015**, *206*, 196–208. [CrossRef] [PubMed]
55. Wong, C.Y.S.; Gamon, J.A. Three causes of variation in the photochemical reflectance index (PRI) in evergreen conifers. *New Phytol.* **2015**, *206*, 187–195. [CrossRef] [PubMed]

56. Drolet, G.G.; Huemmrich, K.F.; Hall, F.G.; Middleton, E.M.; Black, T.A.; Barr, A.G.; Margolis, H.A. A MODIS-derived photochemical reflectance index to detect inter-annual variations in the photosynthetic light-use efficiency of a boreal deciduous forest. *Remote Sens. Environ.* **2005**, *98*, 212–224. [CrossRef]
57. Goerner, A.; Reichstein, M.; Rambal, S. Tracking seasonal drought effects on ecosystem light use efficiency with satellite-based PRI in a Mediterranean forest. *Remote Sens. Environ.* **2009**, *113*, 1101–1111. [CrossRef]
58. Rahman, A.F.; Cordova, V.D.; Gamon, J.A.; Schmid, H.P.; Sims, D.A. Potential of MODIS ocean bands for estimating CO_2 flux from terrestrial vegetation: A novel approach. *Geophys. Res. Lett.* **2004**, *31*, 3–6. [CrossRef]
59. Rahman, A.F.; Gamon, J.A.; Fuentes, D.A.; Roberts, D.A.; Prentiss, D. Modeling spatially distributed ecosystem flux of boreal forest using hyperspectral indices from AVIRIS imagery. *J. Geophys. Res.* **2001**, *106*, 33579–33591. [CrossRef]
60. Stagakis, S.; Markos, N.; Sykioti, O.; Kyparissis, A. Tracking seasonal changes of leaf and canopy light use efficiency in a *Phlomis fruticosa* Mediterranean ecosystem using field measurements and multi-angular satellite hyperspectral imagery. *ISPRS J. Photogramm. Remote Sens.* **2014**, *97*, 138–151. [CrossRef]
61. Gamon, J.A.; Field, C.B.; Goulden, M.L.; Griffin, K.L.; Hartley, A.E.; Joel, G.; Peñuelas, J.; Valentini, R. Relationships Between NDVI, canopy structure, and photosynthesis in three Californian vegetation types. *Ecol. Appl.* **1995**, *21*, 28–41. [CrossRef]
62. Mänd, P.; Hallik, L.; Peñuelas, J.; Nilson, T.; Duce, P.; Emmett, B.A.; Beier, C.; Estiarte, M.; Garadnai, J.; Kalapos, T.; Schmidt, I.K.; Kovács-Láng, E.; Prieto, P.; Tietema, A.; Westerveld, J.W.; Kull, O. Responses of the reflectance indices PRI and NDVI to experimental warming and drought in European shrublands along a north-south climatic gradient. *Remote Sens. Environ.* **2010**, *114*, 626–636. [CrossRef]
63. Stylinski, C.D.; Gamon, J.A.; Oechel, W.C. Seasonal patterns of reflectance indices, carotenoid pigments and photosynthesis of evergreen chaparral species. *Oecologia* **2002**, *131*, 366–374.
64. Drolet, G.G.; Middleton, E.M.; Huemmrich, K.F.; Hall, F.G.; Amiro, B.D.; Barr, A.G.; Black, T.A.; McCaughey, J.H.; Margolis, H.A. Regional mapping of gross light-use efficiency using MODIS spectral indices. *Remote Sens. Environ.* **2008**, *112*, 3064–3078. [CrossRef]
65. Peñuelas, J.; Bartrons, M.; Llusia, J.; Filella, I. Sensing the energetic status of plants and ecosystems. *Trends Plant Sci.* **2015**, *20*, 528–530. [CrossRef] [PubMed]
66. Song, C.; Dannenberg, M.P.; Hwang, T. Optical remote sensing of terrestrial ecosystem primary productivity. *Prog. Phys. Geogr.* **2013**, *37*, 834–854. [CrossRef]
67. Gamon, J.A.; Berry, J.A. Facultative and constitutive pigment effects on the Photochemical Reflectance Index (PRI) in sun and shade conifer needles. *Isr. J. Plant Sci.* **2012**, *60*, 85–95. [CrossRef]
68. Hall, F.G.; Hilker, T.; Coops, N.C.; Lyapustin, A.; Huemmrich, K.F.; Middleton, E.; Margolis, H.; Drolet, G.; Black, T.A. Multi-angle remote sensing of forest light use efficiency by observing PRI variation with canopy shadow fraction. *Remote Sens. Environ.* **2008**, *112*, 3201–3211. [CrossRef]
69. Hernández-Clemente, R.; Navarro-Cerrillo, R.M.; Suárez, L.; Morales, F.; Zarco-Tejada, P.J. Assessing structural effects on PRI for stress detection in conifer forests. *Remote Sens. Environ.* **2011**, *115*, 2360–2375. [CrossRef]
70. Hilker, T.; Lyapustin, A.; Hall, F.G.; Wang, Y.; Coops, N.C.; Drolet, G.; Black, T.A. An assessment of photosynthetic light use efficiency from space: Modeling the atmospheric and directional impacts on PRI reflectance. *Remote Sens. Environ.* **2009**, *113*, 2463–2475. [CrossRef]
71. Hilker, T.; Coops, N.C.; Hall, F.G.; Nichol, C.J.; Lyapustin, A.; Black, T.A.; Wulder, M.A.; Leuning, R.; Barr, A.; Hollinger, D.Y.; et al. Inferring terrestrial photosynthetic light use efficiency of temperate ecosystems from space. *J. Geophys. Res. Biogeosciences* **2011**, *116*, 1–11. [CrossRef]
72. Porcar-Castell, A.; Garcia-Plazaola, J.I.; Nichol, C.J.; Kolari, P.; Olascoaga, B.; Kuusinen, N.; Fernández-Marín, B.; Pulkkinen, M.; Juurola, E.; Nikinmaa, E. Physiology of the seasonal relationship between the photochemical reflectance index and photosynthetic light use efficiency. *Oecologia* **2012**, *170*, 313–323. [CrossRef] [PubMed]
73. Suáez, L.; Zarco-Tejada, P.J.; Sepulcre-Cantó, G.; Pérez-Priego, O.; Miller, J.R.; Jiménez-Muñoz, J.C.; Sobrino, J. Assessing canopy PRI for water stress detection with diurnal airborne imagery. *Remote Sens. Environ.* **2008**, *112*, 560–575.
74. Suárez, L.; Zarco-Tejada, P.J.; Berni, J.A.J.; González-Dugo, V.; Fereres, E. Modelling PRI for water stress detection using radiative transfer models. *Remote Sens. Environ.* **2009**, *113*, 730–744. [CrossRef]

75. Zarco-Tejada, P.J.; González-Dugo, V.; Williams, L.E.; Suárez, L.; Berni, J.A.J.; Goldhamer, D.; Fereres, E. A PRI-based water stress index combining structural and chlorophyll effects: Assessment using diurnal narrow-band airborne imagery and the CWSI thermal index. *Remote Sens. Environ.* **2013**, *138*, 38–50. [CrossRef]
76. Gamon, J.A.; Kovalchuck, O.; Wong, C.Y.S.; Harris, A.; Garrity, S.R. Monitoring seasonal and diurnal changes in photosynthetic pigments with automated PRI and NDVI sensors. *Biogeosciences* **2015**, *12*, 4149–4159. [CrossRef]
77. Nakaji, T.; Kosugi, Y.; Takanashi, S.; Niiyama, K.; Noguchi, S.; Tani, M.; Oguma, H.; Nik, A.R.; Kassim, A.R. Estimation of light-use efficiency through a combinational use of the photochemical reflectance index and vapor pressure deficit in an evergreen tropical rainforest at Pasoh, Peninsular Malaysia. *Remote Sens. Environ.* **2014**, *150*, 82–92. [CrossRef]
78. Guo, J.M.; Trotter, C.M. Estimating photosynthetic light-use efficiency using the photochemical reflectance index: the effects of short-term exposure to elevated CO_2 and low temperature. *Int. J. Remote Sens.* **2006**, *27*, 4677–4684. [CrossRef]
79. Goerner, A.; Reichstein, M.; Tomelleri, E.; Hanan, N.; Rambal, S.; Papale, D.; Dragoni, D.; Schmullius, C. Remote sensing of ecosystem light use efficiency with MODIS-based PRI. *Biogeosciences* **2011**, *8*, 189–202. [CrossRef]
80. Nakaji, T.; Oguma, H.; Fujinuma, Y. Seasonal changes in the relationship between photochemical reflectance index and photosynthetic light use efficiency of Japanese larch needles. *Int. J. Remote Sens.* **2006**, *27*, 493–509. [CrossRef]
81. Cheng, Y.B.; Middleton, E.M.; Zhang, Q.; Huemmrich, K.F.; Campbell, P.K.E.; Corp, L.A.; Cook, B.D.; Kustas, W.P.; Daughtry, C.S. Integrating solar induced fluorescence and the photochemical reflectance index for estimating gross primary production in a cornfield. *Remote Sens.* **2013**, *5*, 6857–6879. [CrossRef]
82. Cheng, Y.B.; Middleton, E.M.; Huemmrich, K.F.; Zhang, Q.; Campbell, P.K.E.; Corp, L.A.; Russ, A.L.; Kustas, W.P. Utilizing in situ directional hyperspectral measurements to validate bio-indicator simulations for a corn crop canopy. *Ecol. Inform.* **2010**, *5*, 330–338. [CrossRef]
83. Cheng, Y.B.; Middleton, E.M.; Zhang, Q.; Corp, L.A.; Dandois, J.; Kustas, W.P. The photochemical reflectance index from directional cornfield reflectances: Observations and simulations. *Remote Sens. Environ.* **2012**, *124*, 444–453. [CrossRef]
84. Gamon, J.A.; Bond, B. Effects of irradiance and photosynthetic downregulation on the photochemical reflectance index in Douglas-fir and ponderosa pine. *Remote Sens. Environ.* **2013**, *135*, 141–149. [CrossRef]
85. Harris, A.; Gamon, J.A.; Pastorello, G.Z.; Wong, C.Y.S. Retrieval of the photochemical reflectance index for assessing xanthophyll cycle activity: A comparison of near-surface optical sensors. *Biogeosciences* **2014**, *11*, 6277–6292. [CrossRef]
86. Hmimina, G.; Dufrêne, E.; Soudani, K. Relationship between photochemical reflectance index and leaf ecophysiological and biochemical parameters under two different water statuses: Towards a rapid and efficient correction method using real-time measurements. *Plant Cell Environ.* **2014**, *37*, 473–487. [CrossRef] [PubMed]
87. Weng, J.H.; Jhaung, L.H.; Lin, R.J.; Chen, H.Y. Relationship between photochemical efficiency of photosystem II and the photochemical reflectance index of mango tree: Merging data from different illuminations, seasons and leaf colors. *Tree Physiol.* **2010**, *30*, 469–478. [CrossRef] [PubMed]
88. Rahimzadeh-Bajgiran, P.; Munehiro, M.; Omasa, K. Relationships between the photochemical reflectance index (PRI) and chlorophyll fluorescence parameters and plant pigment indices at different leaf growth stages. *Photosynth. Res.* **2012**, *113*, 261–271. [CrossRef] [PubMed]
89. Ibaraki, Y.; Gupta, S.D. Nondestructive evaluation of the photosynthetic properties of micropropagated plantlets by imaging photochemical reflectance index under low light intensity. *In Vitro Cell. Dev. Biol. Plant* **2010**, *46*, 530–536. [CrossRef]
90. Sarlikioti, V.; Driever, S.M.; Marcelis, L.F.M. Photochemical reflectance index as a mean of monitoring early water stress. *Ann. Appl. Biol.* **2010**, *157*, 81–89. [CrossRef]
91. Magney, T.S.; Eusden, S.A.; Eitel, J.U.H.; Logan, B.A.; Jiang, J.; Vierling, L.A. Assessing leaf photoprotective mechanisms using terrestrial LiDAR: Towards mapping canopy photosynthetic performance in three dimensions. *New Phytol.* **2014**, *201*, 344–356. [CrossRef] [PubMed]

92. Kováč, D.; Malenovský, Z.; Urban, O.; Špunda, V.; Kalina, J.; Ač, A.; Kaplan, V.; Hanuš, J. Response of green reflectance continuum removal index to the xanthophyll de-epoxidation cycle in Norway spruce needles. *J. Exp. Bot.* **2013**, *64*, 1817–1827. [CrossRef] [PubMed]
93. Osório, J.; Osório, M.L.; Romano, A. Reflectance indices as nondestructive indicators of the physiological status of *Ceratonia siliqua* seedlings under varying moisture and temperature regimes. *Funct. Plant Biol.* **2012**, *39*, 588–597. [CrossRef]
94. Shrestha, S.; Brueck, H.; Asch, F. Chlorophyll index, photochemical reflectance index and chlorophyll fluorescence measurements of rice leaves supplied with different N levels. *J. Photochem. Photobiol. B Biol.* **2012**, *113*, 7–13. [CrossRef] [PubMed]
95. Su, Y.; Zhang, Z.; Su, G.; Liu, J.; Liu, C.; Shi, G. Genotypic differences in spectral and photosynthetic response of peanut to iron deficiency. *J. Plant Nutr.* **2015**, *38*, 145–160. [CrossRef]
96. Rajsnerová, P.; Klem, K.; Holub, P.; Novotná, K.; Večeřová, K.; Kozáčiková, M.; Rivas-Ubach, A.; Sardans, J.; Marek, M.V.; Peñuelas, J.; Urban, O. Morphological, biochemical and physiological traits of upper and lower canopy leaves of European beech tend to converge with increasing altitude. *Tree Physiol.* **2015**, *35*, 47–60. [CrossRef] [PubMed]
97. Lv, Z.; Zhang, X.; Liu, L.; Guo, Y.; Fan, Y.; Yang, X.; Li, Y.; Zhang, W. Comparing intraspecific responses of 12 winter wheat cultivars to different doses of ultraviolet-B radiation. *J. Photochem. Photobiol. B Biol.* **2013**, *119*, 1–8. [CrossRef] [PubMed]
98. Pallozzi, E.; Fortunati, A.; Marino, G.; Loreto, F.; Agati, G.; Centritto, M. BVOC emission from *Populus* × *canadensis* saplings in response to acute UV-A radiation. *Physiol. Plant.* **2013**, *148*, 51–61. [CrossRef] [PubMed]
99. Ashourloo, D.; Mobasheri, M.R.; Huete, A. Evaluating the effect of different wheat rust disease symptoms on vegetation indices using hyperspectral measurements. *Remote Sens.* **2014**, *6*, 5107–5123. [CrossRef]
100. Ashourloo, D.; Mobasheri, M.R.; Huete, A. Developing two spectral disease indices for detection of wheat leaf rust (*Pucciniatriticina*). *Remote Sens.* **2014**, *6*, 4723–4740. [CrossRef]
101. Calderón, R.; Navas-Cortés, J.A.; Lucena, C.; Zarco-Tejada, P.J. High-resolution airborne hyperspectral and thermal imagery for early detection of *Verticillium* wilt of olive using fluorescence, temperature and narrow-band spectral indices. *Remote Sens. Environ.* **2013**, *139*, 231–245. [CrossRef]
102. Elena, G.; Fernàndez-Martínez, J.; Zacchini, M.; Moret, A.; Fleck, I. Susceptibility to melampsora leaf rust of poplar clones from diverse genetic backgrounds: Effects on photochemistry and water relations. *J. Plant Stud.* **2014**, *3*, 1–12. [CrossRef]
103. Xue, Z.; Gao, H.; Zhao, S. Effects of cadmium on the photosynthetic activity in mature and young leaves of soybean plants. *Environ. Sci. Pollut. Res.* **2014**, *21*, 4656–4664. [CrossRef] [PubMed]
104. Mõttus, M.; Rautiainen, M. Scaling PRI between coniferous canopy structures. *IEEE J. Sel. Top. Appl. Earth Obs. Remote Sens.* **2013**, *6*, 708–714. [CrossRef]
105. Garrity, S.R.; Eitel, J.U.H.; Vierling, L.A. Disentangling the relationships between plant pigments and the photochemical reflectance index reveals a new approach for remote estimation of carotenoid content. *Remote Sens. Environ.* **2011**, *115*, 628–635. [CrossRef]
106. Cogliati, S.; Rossini, M.; Julitta, T.; Meroni, M.; Schickling, A.; Burkart, A.; Pinto, F.; Rascher, U.; Colombo, R. Continuous and long-term measurements of reflectance and sun-induced chlorophyll fluorescence by using novel automated field spectroscopy systems. *Remote Sens. Environ.* **2015**, *164*, 270–281. [CrossRef]
107. Hmimina, G.; Merlier, E.; Dufrêne, E.; Soudani, K. Deconvolution of pigment and physiologically related photochemical reflectance index variability at the canopy scale over an entire growing season. *Plant Cell Environ.* **2015**, *38*, 1578–1590. [CrossRef] [PubMed]
108. Damm, A.; Guanter, L.; Verhoef, W.; Schläpfer, D.; Garbari, S.; Schaepman, M.E. Impact of varying irradiance on vegetation indices and chlorophyll fluorescence derived from spectroscopy data. *Remote Sens. Environ.* **2015**, *156*, 202–215. [CrossRef]
109. Wu, C.; Niu, Z.; Tang, Q.; Huang, W. Revised photochemical reflectance index (PRI) for predicting light use efficiency of wheat in a growth cycle: Validation and comparison. *Int. J. Remote Sens.* **2010**, *31*, 2911–2924. [CrossRef]
110. Liu, L.; Zhang, Y.; Jiao, Q.; Peng, D. Assessing photosynthetic light-use efficiency using a solar-induced chlorophyll fluorescence and photochemical reflectance index. *Int. J. Remote Sens.* **2013**, *34*, 4264–4280. [CrossRef]

111. Zinnert, J.C.; Nelson, J.D.; Hoffman, A.M. Effects of salinity on physiological responses and the photochemical reflectance index in two co-occurring coastal shrubs. *Plant Soil* **2012**, *354*, 45–55. [CrossRef]
112. Harris, A.; Owen, S.M.; Sleep, D.; Pereira, M.D. Constitutive changes in pigment concentrations: implications for estimating isoprene emissions using the photochemical reflectance index. *Physiol. Plant.* **2016**, *156*, 190–200. [CrossRef] [PubMed]
113. Weng, J.H.; Wong, S.L.; Lai, K.M.; Lin, R.J. Relationships between photosystem II efficiency and photochemical reflectance index under different levels of illumination: Comparison among species grown at high- and low elevations through different seasons. *Trees-Struct. Funct.* **2012**, *26*, 343–351. [CrossRef]
114. Nyongesah, M.J.; Wang, Q.; Li, P. Effectiveness of photochemical reflectance index to trace vertical and seasonal chlorophyll a/b ratio in *Haloxylon ammodendron*. *Acta Physiol. Plant.* **2015**, *37*. [CrossRef]
115. Ainsworth, E.A.; Serbin, S.P.; Skoneczka, J.A.; Townsend, P.A. Using leaf optical properties to detect ozone effects on foliar biochemistry. *Photosynth. Res.* **2014**, *119*, 65–76. [CrossRef] [PubMed]
116. Ghulam, A.; Fishman, J.; Maimaitiyiming, M.; Wilkins, J.L.; Maimaitijiang, M.; Welsh, J.; Bira, B.; Grzovic, M. Characterizing crop responses to background ozone in open-air agricultural field by using reflectance spectroscopy. *IEEE Geosci. Remote Sens. Lett.* **2015**, *12*, 1307–1311. [CrossRef]
117. Hernández-Clemente, R.; Navarro-Cerrillo, R.M.; Zarco-Tejada, P.J. Carotenoid content estimation in a heterogeneous conifer forest using narrow-band indices and PROSPECT + DART simulations. *Remote Sens. Environ.* **2012**, *127*, 298–315. [CrossRef]
118. Barták, M.; Trnková, K.; Hansen, E.S.; Hazdrová, J.; Skácelová, K.; Hájek, J.; Forbelská, M. Effect of dehydration on spectral reflectance and photosynthetic efficiency in *Umbilicaria arctica* and *U. hyperborea*. *Biol. Plant.* **2015**, *59*, 357–365. [CrossRef]
119. Sun, P.; Wahbi, S.; Tsonev, T.; Haworth, M.; Liu, S.; Centritto, M. On the use of leaf spectral indices to assess water status and photosynthetic limitations in *Olea europaea* L. during water-stress and recovery. *PLoS ONE* **2014**, *9*, e105165. [CrossRef] [PubMed]
120. Zarco-Tejada, P.J.; González-Dugo, V.; Berni, J.A.J. Fluorescence, temperature and narrow-band indices acquired from a UAV platform for water stress detection using a micro-hyperspectral imager and a thermal camera. *Remote Sens. Environ.* **2012**, *117*, 322–337. [CrossRef]
121. Tsonev, T.; Wahbi, S.; Sun, P.; Sorrentino, G.; Centritto, M. Gas exchange, water relations and their relationships with photochemical reflectance index in *Quercus ilex* plants during water stress and recovery. *Int. J. Agric. Biol.* **2014**, *16*, 335–341.
122. Naumann, J.C.; Bissett, S.N.; Young, D.R.; Edwards, J.; Anderson, J.E. Diurnal patterns of photosynthesis, chlorophyll fluorescence, and PRI to evaluate water stress in the invasive species, *Elaeagnus umbellata* Thunb. *Trees-Struct. Funct.* **2010**, *24*, 237–245. [CrossRef]
123. Soudani, K.; Hmimina, G.; Dufrêne, E.; Berveiller, D.; Delpierre, N.; Ourcival, J.M.; Rambal, S.; Joffre, R. Relationships between photochemical reflectance index and light-use efficiency in deciduous and evergreen broadleaf forests. *Remote Sens. Environ.* **2014**, *144*, 73–84. [CrossRef]
124. Wu, C.; Huang, W.; Yang, Q.; Xie, Q. Improved estimation of light use efficiency by removal of canopy structural effect from the photochemical reflectance index (PRI). *Agric. Ecosyst. Environ.* **2015**, *199*, 333–338. [CrossRef]
125. Marino, G.; Pallozzi, E.; Cocozza, C.; Tognetti, R.; Giovannelli, A.; Cantini, C.; Centritto, M. Assessing gas exchange, sap flow and water relations using tree canopy spectral reflectance indices in irrigated and rainfed *Olea europaea* L. *Environ. Exp. Bot.* **2014**, *99*, 43–52. [CrossRef]
126. Stagakis, S.; González-Dugo, V.; Cid, P.; Guillén-Climent, M.L.; Zarco-Tejada, P.J. Monitoring water stress and fruit quality in an orange orchard under regulated deficit irrigation using narrow-band structural and physiological remote sensing indices. *ISPRS J. Photogramm. Remote Sens.* **2012**, *71*, 47–61. [CrossRef]
127. Gray, S.B.; Dermody, O.; DeLucia, E.H. Spectral reflectance from a soybean canopy exposed to elevated CO_2 and O_3. *J. Exp. Bot.* **2010**, *61*, 4413–4422. [CrossRef] [PubMed]
128. Suárez, L.; Zarco-Tejada, P.J.; Gonzáez-Dugo, V.; Berni, J.A.J.; Sagardoy, R.; Morales, F.; Fereres, E. Detecting water stress effects on fruit quality in orchards with time-series PRI airborne imagery. *Remote Sens. Environ.* **2010**, *114*, 286–298. [CrossRef]
129. Rossini, M.; Meroni, M.; Migliavacca, M.; Manca, G.; Cogliati, S.; Busetto, L.; Picchi, V.; Cescatti, A.; Seufert, G.; Colombo, R. High resolution field spectroscopy measurements for estimating gross ecosystem production in a rice field. *Agric. For. Meteorol.* **2010**, *150*, 1283–1296. [CrossRef]

130. Van Leeuwen, M.; Kremens, R.L.; van Aardt, J. Tracking diurnal variation in photosynthetic down-regulation using low cost spectroscopic instrumentation. *Sensors* **2015**, *15*, 10616–10630. [CrossRef] [PubMed]
131. Middleton, E.M.; Huemmrich, K.F.; Cheng, Y.B.; Margolis, H.A. Spectral bioindicators of photosynthetic efficiency and vegetation stress. In *Hyperspectral Remote Sensing of Vegetation*; CRC Press: Boca Raton, FL, USA, 2011; pp. 265–288.
132. Stagakis, S.; Markos, N.; Sykioti, O.; Kyparissis, A. Monitoring canopy biophysical and biochemical parameters in ecosystem scale using satellite hyperspectral imagery: An application on a *Phlomis fruticosa* Mediterranean ecosystem using multiangular CHRIS/PROBA observations. *Remote Sens. Environ.* **2010**, *114*, 977–994. [CrossRef]
133. Galvão, L.S.; Breunig, F.M.; dos Santos, J.R.; de Moura, Y.M. View-illumination effects on hyperspectral vegetation indices in the Amazonian tropical forest. *Int. J. Appl. Earth Obs. Geoinf.* **2013**, *21*, 291–300. [CrossRef]
134. Sims, D.A.; Rahman, A.F.; Vermote, E.F.; Jiang, Z. Seasonal and inter-annual variation in view angle effects on MODIS vegetation indices at three forest sites. *Remote Sens. Environ.* **2011**, *115*, 3112–3120. [CrossRef]
135. Vicca, S.; Balzarolo, M.; Filella, I.; Granier, A.; Herbst, M.; Knohl, A.; Longdoz, B.; Mund, M.; Nagy, Z.; Pintér, K.; et al. Remotely-sensed detection of effects of extreme droughts on gross primary production. *Sci. Rep.* **2016**, *6*, 1–13. [CrossRef] [PubMed]
136. Rossini, M.; Cogliati, S.; Meroni, M.; Migliavacca, M.; Galvagno, M.; Busetto, L.; Cremonese, E.; Julitta, T.; Siniscalco, C.; Morra Di Cella, U.; et al. Remote sensing-based estimation of gross primary production in a subalpine grassland. *Biogeosciences* **2012**, *9*, 2565–2584. [CrossRef]
137. Drolet, G.; Wade, T.; Nichol, C.J.; MacLellan, C.; Levula, J.; Porcar-Castell, A.; Nikinmaa, E.; Vesala, T. A temperature-controlled spectrometer system for continuous and unattended measurements of canopy spectral radiance and reflectance. *Int. J. Remote Sens.* **2014**, *35*, 1769–1785. [CrossRef]
138. Gamon, J.A.; Rahman, A.F.; Dungan, J.L.; Schildhauer, M.; Huemmrich, K.F. Spectral Network (SpecNet)—What is it and why do we need it? *Remote Sens. Environ.* **2006**, *103*, 227–235. [CrossRef]
139. Pacheco-Labrador, J.; Martín, M.P. Nonlinear response in a field portable spectroradiometer: Characterization and effects on output reflectance. *IEEE Trans. Geosci. Remote Sens.* **2014**, *52*, 920–928. [CrossRef]
140. Ibaraki, Y.; Matsumura, K.; Dutta Gupta, S. Low-cost photochemical reflectance index measurements of micropropagated plantlets using image analysis. *Comput. Electron. Agric.* **2010**, *71*, 170–175. [CrossRef]
141. Peñuelas, J.; Marino, G.; Llusia, J.; Morfopoulos, C.; Farré-Armengol, G.; Filella, I. Photochemical reflectance index as an indirect estimator of foliar isoprenoid emissions at the ecosystem level. *Nat. Commun.* **2013**, *4*, 2604. [CrossRef] [PubMed]
142. Stratoulias, D.; Balzter, H.; Zlinszky, A.; Tóth, V.R. Assessment of ecophysiology of lake shore reed vegetation based on chlorophyll fluorescence, field spectroscopy and hyperspectral airborne imagery. *Remote Sens. Environ.* **2015**, *157*, 72–84. [CrossRef]
143. Sun, C.X.; Yuan, F.; Zhang, Y.L.; Cui, Z.B.; Chen, Z.H.; Chen, L.J.; Wu, Z.J. Unintended effects of genetic transformation on photosynthetic gas exchange, leaf reflectance and plant growth properties in barley (*Hordeum vulgare* L.). *Photosynthetica* **2013**, *51*, 22–32. [CrossRef]
144. Yoshizumi, Y.; Li, M.S.; Akihiro, I. Assessment of photochemical reflectance index as a tool for evaluation of chlorophyll fluorescence parameters in cotton and peanut cultivars under water stress condition. *Agric. Sci. China* **2010**, *9*, 662–670.
145. Šebela, D.; Quiñones, C.; Olejníčková, J.; Jagadish, K.S.V. Temporal chlorophyll fluorescence signals to track changes in optical properties of maturing rice panicles exposed to high night temperature. *Field Crop. Res.* **2015**, *177*, 75–85. [CrossRef]
146. Delalieux, S.; Zarco-tejada, P.J.; Somers, B.; Delalieux, S.; Zarco-tejada, P.J.; Tits, L.; Ángel, M.; Bello, J.; Intrigliolo, D.S.; Somers, B. Unmixing-based fusion of hyperspatial and hyperspectral airborne imagery for early detection of vegetation stress. *IEEE J. Sel. Top. Appl. Earth Obs. Remote Sens.* **2014**, *7*, 2571–2582. [CrossRef]
147. Rossini, M.; Panigada, C.; Cilia, C.; Meroni, M.; Busetto, L.; Cogliati, S.; Amaducci, S.; Colombo, R. Discriminating irrigated and rainfed maize with diurnal fluorescence and canopy temperature airborne maps. *ISPRS Int. J. Geo-Inf.* **2015**, *4*, 626–646. [CrossRef]

148. Panigada, C.; Rossini, M.; Meroni, M.; Cilia, C.; Busetto, L.; Amaducci, S.; Boschetti, M.; Cogliati, S.; Picchi, V.; Pinto, F.; et al. Fluorescence, PRI and canopy temperature for water stress detection in cereal crops. *Int. J. Appl. Earth Obs. Geoinf.* **2014**, *30*, 167–178. [CrossRef]
149. Zarco-Tejada, P.J.; Morales, A.; Testi, L.; Villalobos, F.J. Spatio-temporal patterns of chlorophyll fluorescence and physiological and structural indices acquired from hyperspectral imagery as compared with carbon fluxes measured with eddy covariance. *Remote Sens. Environ.* **2013**, *133*, 102–115. [CrossRef]
150. Rossini, M.; Fava, F.; Cogliati, S.; Meroni, M.; Marchesi, A.; Panigada, C.; Giardino, C.; Busetto, L.; Migliavacca, M.; Amaducci, S.; et al. Assessing canopy PRI from airborne imagery to map water stress in maize. *ISPRS J. Photogramm. Remote Sens.* **2013**, *86*, 168–177. [CrossRef]
151. Hall, F.G.; Hilker, T.; Coops, N.C. PHOTOSYNSAT, photosynthesis from space: Theoretical foundations of a satellite concept and validation from tower and spaceborne data. *Remote Sens. Environ.* **2011**, *115*, 1918–1925. [CrossRef]
152. Kefauver, S.C.; Peñuelas, J.; Ustin, S. Using topographic and remotely sensed variables to assess ozone injury to conifers in the Sierra Nevada (USA) and Catalonia (Spain). *Remote Sens. Environ.* **2013**, *139*, 138–148. [CrossRef]
153. Balzarolo, M.; Vescovo, L.; Hammerle, A.; Gianelle, D.; Papale, D.; Wohlfahrt, G. On the relationship between ecosystem-scale hyperspectral reflectance and CO_2 exchange in European mountain grasslands. *Biogeosci. Discuss.* **2015**, *11*, 10323–10363. [CrossRef]
154. Hilker, T.; Hall, F.G.; Tucker, C.J.; Coops, N.C.; Black, T.A.; Nichol, C.J.; Sellers, P.J.; Barr, A.; Hollinger, D.Y.; Munger, J.W. Data assimilation of photosynthetic light-use efficiency using multi-angular satellite data: II Model implementation and validation. *Remote Sens. Environ.* **2012**, *121*, 287–300. [CrossRef]
155. Garrity, S.R.; Vierling, L.A.; Bickford, K. A simple filtered photodiode instrument for continuous measurement of narrowband NDVI and PRI over vegetated canopies. *Agric. For. Meteorol.* **2010**, *150*, 489–496. [CrossRef]
156. Roujean, J.L.; Breon, F.M. Estimating PAR absorbed by vegetation from bidirectional reflectance measurements. *Remote Sens. Environ.* **1995**, *51*, 375–384. [CrossRef]
157. Meroni, M.; Rossini, M.; Guanter, L.; Alonso, L.; Rascher, U.; Colombo, R.; Moreno, J. Remote sensing of solar-induced chlorophyll fluorescence: Review of methods and applications. *Remote Sens. Environ.* **2009**, *113*, 2037–2051. [CrossRef]
158. Porcar-Castell, A.; Tyystjärvi, E.; Atherton, J.; Van Der Tol, C.; Flexas, J.; Pfündel, E.E.; Moreno, J.; Frankenberg, C.; Berry, J.A. Linking chlorophyll a fluorescence to photosynthesis for remote sensing applications: Mechanisms and challenges. *J. Exp. Bot.* **2014**, *65*, 4065–4095. [CrossRef] [PubMed]
159. Brugnoli, E.; Björkman, O. Chloroplast movements in leaves: influence on chlorophyll fluorescence and measurements of light-induced absorbance changes related to ΔpH and zeaxanthin formation. *Photosynth. Res.* **1992**, *32*, 23–35. [CrossRef] [PubMed]
160. Gago, J.; Douthe, C.; Coopman, R.E.; Gallego, P.P.; Ribas-Carbo, M.; Flexas, J.; Escalona, J.; Medrano, H. UAVs challenge to assess water stress for sustainable agriculture. *Agric. Water Manag.* **2015**, *153*, 9–19. [CrossRef]
161. Sentinel Online—ESA. Available online: https://sentinel.esa.int/web/sentinel/home (accessed on 23 June 2016).
162. EnMAP. Available online: www.enmap.org (accessed on 23 June 2016).
163. WMO OSCAR—Space-Based Capabilities—Instruments: DESIS. Available online: https://www.wmo-sat.info/oscar/instruments/view/1082 (accessed on 23 June 2016).
164. HyspIRI Mission Study Website. Available online: https://hyspiri.jpl.nasa.gov (accessed on 23 June 2016).
165. Turtle, E.P.; McEwen, A.S.; Collins, G.C.; Fletcher, L.; Hansen, C.J.; Hayes, A.G.; Hurford, T.A.; Kirk, R.L.; Mlinar, A.C.B.; Nimmo, F.; et al. The europa imaging system (EIS): High-resolution imaging and topography to investigate Europa's geology, ice shell, and potential for current activity. *Lunar Planet. Sci. Conf.* **2016**, *47*, 1626.
166. Fluxnet. Available online: https://fluxnet.ornl.gov (accessed on 23 June 2016).